Master's Thesis

SAR Evaluation in Multi-Antenna Mobile Handsets

Apostolos Tsiaras

Department of Electrical and Information Technology,
Faculty of Engineering, LTH, Lund University, March 2014

Master's Thesis

SAR Evaluation in Multi-Antenna Mobile Handsets

By

Apostolos Tsiaras

Department of Electrical and Information Technology
Faculty of Engineering, LTH, Lund University
SE-221 00 Lund, Sweden,

March 2014

Abstract

Multiple antennas are widely used in mobile terminals to provide high data transmission rates. However, due to the presence of many antenna elements, the radiation performance of the antenna system becomes more sensitive to user proximity. The user head and hand, which are in the reactive near field of the mobile handset antennas, can significantly influence the antenna impedances, radiation patterns, efficiencies and current coupling between the antenna elements. Human tissues, as lossy dielectric materials at mobile phone frequencies, absorb radio frequency (RF) power. As a measure of the rate at which energy is absorbed by a body, Specific Absorption Rate (SAR) is used to evaluate the exposure of the body to an RF electromagnetic field. SAR is defined as the power absorbed per mass of tissue and has the unit of watts per kilogram. As is the case with single antenna devices, multiple-input multiple-output (MIMO) enabled devices should also be required to comply with certain standards for limiting human exposure to RF fields. However, from the antenna design perspective, there is a lack of systematic study on how to reduce SAR, particularly for multi-antennas.

The goal of this Master thesis is to analyze the impact of different antenna factors on SAR in multi-antenna mobile handsets. The dependence of MIMO SAR on different antenna types, antenna locations and chassis excitations, has been studied. Another purpose of the work is to propose some methods for MIMO SAR evaluation.

“Αυτή η εργασία είναι αφιερωμένη στους γονείς μου, Κώστα και Ξανθή. Χωρίς την αμέριστη υποστήριξή τους όλα αυτά θα ήταν για εμένα ένα όνειρο.”

Acknowledgments

I would like to express my deep gratitude to Associate Professor Dr. *Buon Kiong Lau* for giving me the opportunity to perform my thesis project under his guidance, and introducing me to a team of highly capable and enthusiastic young researchers. His valuable suggestions were not only limited to research or technological aspects but they also included advices for my future career as well.

My grateful thanks are certainly extended to Dr. *Hui Li*, my thesis supervisor. Her help during the planning and development of this project has been priceless and her willingness to provide me assistance whenever I was facing difficulties is deeply appreciated. Despite working alone in this project it never felt like so, as a result of her encouragement and effort.

I would also like to express my very great appreciation for the assistance given by Ph.D. candidates *Ivaylo Vasilev* for his help during the fabrication of the prototypes and *Zachary Miers* for our discussions about antenna design and simulation challenges. Thank you both for all the fruitful conversations.

Furthermore, I am most grateful to Dr. *Benoît Derat*, President of ART-FI SAS for hosting me in his company during the measurement campaign. His valuable recommendations and constructive suggestions radically improved this report. I also thank COST Action IC1004 for financially supporting the measurement campaign with a Short Term Scientific Mission (STSM) Grant (Grant No. COST-STSM-IC1004-14193).

Finally many thanks go to my colleagues and friends from the International Master Program in Wireless Communications (Class of 2011-2013) for teaching me the benefits of diversity from a human perspective. Being exposed in such a big blend of cultures and ideas has been one of the best experiences of my life.

Table of Contents

CHAPTER 1

1 Introduction

1.1 Preface

The big proliferation of mobile communication systems increased the concern on how the human body and the antenna(s) in a mobile phone interact. There are two important aspects to take into account: The influence of the human body (head and hand are usually in the reactive near field of the antenna) on the radiation properties of the mobile phone is the first aspect. In general, the proximity of the human body to the antenna degrades the antenna's performance. Antenna characteristics that are mostly affected by the presence of the human body are radiation pattern, input impedance and radiation efficiency. The second aspect can be considered more critical from the human perspective; it is about how the mobile phone antenna interacts with the human body. When a mobile phone operates, part of the radiated power is absorbed by the human tissue. Usually, almost half of the radiated power is dissipated into such tissues as the ear, scalp and brain [1].

At mobile phone frequencies, the body behaves as lossy dielectric material and absorbs RF power. The kinetic energy inside the human tissue increases as a function of time when the microwave energy is dissipated within. If this energy is sufficiently high, the temperature will linearly increase and the rate of this rise is determined by the power deposition. If the frequencies of the mobile phone are close to the resonance frequency of the tissue, then more heat is transmitted to the human body [2], which is mainly composed of water, electrolytes and complex molecules [3]. Thermal effects such as dielectric heating are the obvious effect of electromagnetic (EM) waves. Other effects that might be caused by temporal exposure to EM waves can be headache and nausea. As a measure of the rate at which energy is absorbed by the body, **Specific Absorption Rate** (SAR) is defined as a metric to quantify the exposure of body to an RF electromagnetic field (see Chapter 2 for details).

Multiple Input-Multiple Output (MIMO) system refers to the use of many antennas at the radio transmitter and receiver to improve the performance of a wireless communication link. In recent technology standards like IEEE 802.11n (WiFi), IEEE 802.16 (WiMAX), 3GPP Rel. 7 (HSPA+) and 3GPP Rel. 8 (LTE) - 3GPP Rel. 10 (LTE-Advanced), MIMO has been keenly adopted. MIMO is now widely deployed in mobile devices, but existing exposure guidelines still focus on methodology for single-antenna evaluation. This is because the current use of MIMO technology is mostly in the downlink, and in the uplink only one antenna is used for transmission. The single uplink antenna can either be fixed to one antenna, or it can be chosen based on some criterion, which is referred to as selection diversity. However, the recently deployed LTE-Advanced systems include the feature to provide simultaneous uplink transmission of several data streams from the multiple antennas in the terminal. This scheme is noted as spatial multiplexing (SM). While SAR evaluation for traditional single antennas has been well studied, SAR evaluation for multi-antennas is still under development. For compact MIMO enabled terminal devices, strong mutual coupling between antenna elements can influence the SAR behavior. In this work we aim to study how SAR behaves in uplink MIMO transmissions involving SM. Simultaneous SAR is used as the metric. In the following chapters, we will also study stand-alone SAR, which is used to describe the SAR value in single-antenna uplink transmissions (e.g. using the diversity scheme). Simultaneous SAR and stand-alone SAR will be defined in Chapter 2.

1.2 Objectives

Since the dielectric properties of human tissue can be considered homogeneous, the SAR value is mainly influenced by the electric field (*E*-Field) generated by the antennas and their position relative to the human body. This thesis aims to investigate the influence of different antenna types, antenna locations and chassis excitation on the distributions of electric field and SAR values by utilizing different dual-antenna mobile handsets. Techniques to suppress *E*-Field in the users are also studied. In this way, we can optimize SAR value from the antenna design perspective. Moreover, methods for evaluating SAR in MIMO operation are examined. Seven dual-element MIMO antennas are studied. The SAR spatial distributions and values are evaluated and analyzed by simulations with CST Microwave Studio and then four prototypes are fabricated. SAR measurements of the fabricated handsets are performed in COMOSAR, a state-of-the-art robot SAR measurement system from SATIMO, and then compared with the simulated results.

1.3 Organization

This thesis is organized as follows:

- In Chapter 2, theoretical background on both SAR and MIMO technology is given along with the motivation on how the different MIMO operation modes can affect the overall SAR behavior.
- Chapter 3 presents the antenna configurations and design aspects of a dual antenna mobile device and the challenges that come along when many antennas are used in the same device. A brief overview of the prototypes is also given in this chapter, together with a motivation on the choice of these prototypes for this study.
- In Chapter 4, the details of each mobile handset are presented in terms of antenna design and scattering parameters.
- Chapter 5 presents the antenna and simulation setups in the CST software, such as the reference power, target frequencies and the distance between the prototypes and the phantom.
- A detailed study for the “Body-Worn Mode” is evaluated through simulations in CST and the results are presented in Chapter 6. This corresponds to the case where a user places his mobile phone in a pocket. It is more intuitive to study SAR in this user mode due to the geometrical uniformity of the flat phantom. Comparison of different set-ups and result analysis for several study cases are also presented in this chapter.
- Measurements on the flat phantom with COMOSAR (a robotic near-field SAR measurement system provided by ART-FI) for one fabricated prototype are performed and presented in Chapter 7. The measured results are compared with the simulation results.
- In Chapter 8, four of the prototypes are simulated and analyzed in the “Talking Mode”.
- The conclusions are given in Chapter 9, and plans for future work are also provided.

CHAPTER 2

2 Theoretical Background

2.1 Specific Absorption Rate (SAR)

2.1.1 SAR Definition

The physical interaction of an RF EM wave with a biological material is complex, and it results in an inhomogeneous distribution of the induced EM field and the current density within the human tissue, despite the uniformity of the external exposure field. The important fact that leads to a straightforward definition of the exposure parameter of relevance is the observation that only the EM energy absorbed by the human body can cause a bio effect. Since the radiating part of the mobile phone and the human tissue (hand-head) are only a few millimeters apart in real usage, the evaluation of the exposure of a human in the near field of RF sources makes sense and it is accomplished by measuring the *E*-Field inside the body [3].

Specific Absorption Rate is a measure of the rate at which EM energy is absorbed or dissipated in an element of biological body mass when it is exposed to an RF field from a radiating device. It is defined as:

$$SAR = \frac{\sigma E^2}{2\rho} \ [W/Kg] \qquad (1)$$

σ: is the conductivity of human tissue [S/m] (siemens per meter)
E: is the induced electric field inside the human body [V/m] (volts per meter)
ρ*:* is the density of the tissue sample [kg/m^3] (Kilogram per cubic meter)

SAR is used for the frequency range between 100 KHz and 10GHz and it depends on the geometry of the body part exposed to the EM waves and the location of the source of the energy [5]. The design of a device as well as its operational frequency, antenna input power and orientation with respect to the body are important factors that affect SAR.

2.1.2 SAR Specifications and Standards

Different standards set different SAR threshold values to limit the potential health risk from EM radiation from mobile terminals. The maximum power deposition expressed in SAR, allowed by the FCC is 1.6 W/kg in 1g of tissue from exposure to cellular telephone radiation (US and Canada). On the other hand, the International Commission on Non-Ionizing Radiation Protection (ICNIRP) guidelines stipulate a maximum SAR of 2 W/kg in any 10 g of tissue in the head (EU, Japan and Brazil) [1].

Table 1 : SAR Limit Recommendations

US and Canada (FCC)	EU, Japan and Brazil (ICNIRP)
1.6 W/kg in 1g of tissue	2 W/kg in 10g of tissue

SAR is a point quality and its value varies from one location to the other. Tissue density, conductivity and most significantly the *E*-Field are key parameters that determine the reliability and accuracy of a given SAR value. Normally, the average SAR is considered. We can see from Fig. 1 that the volume of interest is a cube around a point that expands in isotropic directions along the coordinate system until it contains 1g or 10g of tissue, and SAR values are then averaged in the cube.

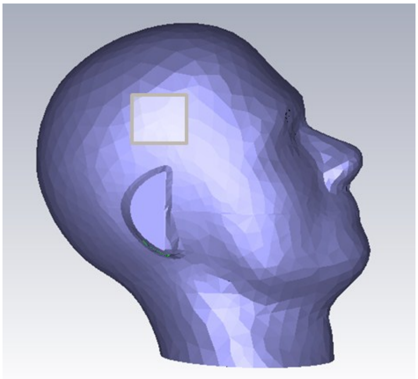

Figure 1: 1/10g SAR
Method: Divide the volume of the human tissue in 1 or 10 grams and integrate the SAR values inside each cube

Comparing the FCC and ICNIRP standards for maximum of mass averaged SAR, it is worth mentioning that the volume of tissue used to define SAR can greatly influence the SAR values. If the absorbed energy is averaged over a defined tissue of 10g, the result may be less strict comparing with the 1g averaged SAR. The latter performs more precise representation of the localized microwave energy absorption and a better measure of SAR distribution inside the head. Thus, in this thesis we will use the FCC limit recommendation, i.e., 1.6 W/kg over 1 g of tissue, since it is a stricter criterion.

2.2 MIMO

The idea of using many antennas at the transmitter (Tx) and the receiver (Rx) in a communication link is to take advantage of the multipath environment in a communication link and allow the system to have many independent channels. It can increase the channel capacity without sacrificing additional frequency spectrum and transmit power.

Figure 2 : Illustration of MIMO technology in modern cellular communications

However, implementing multiple antennas in compact terminal devices such as mobile phones is challenging. Due to the lack of available space in the mobile terminal and the chassis excitation effect, the use of many radiating elements usually causes high mutual coupling among the antennas [3].

2.3 SAR Consideration for MIMO

Same as the single-antenna terminal, the MIMO enabled devices are also required to comply with standards or internationally recognized guidelines for limiting human exposure to RF fields. However, for terminals consisting of more than one antenna in a mobile handset, the influential factors are more complicated than those for traditional single-antenna SAR. Two terms to characterize SAR in MIMO devices are discussed in the following.

2.3.1 Stand-Alone SAR

While MIMO technology is already implemented in the current generation of cellular telecommunication protocols (e.g., LTE), it is mostly used in the downlink. That is to say, in the terminal, multiple antennas are only used in downlink, and only one antenna is used for the uplink, which can be chosen based on the selection diversity scheme. In this scheme, each antenna is always excited separately, and hence the SAR value is obtained separately for each antenna. SAR obtained in this way is called Stand-Alone SAR (SA-SAR) (Fig. 3). This method differs from the single-antenna SAR because when one antenna is used in the handset there is no coupling between the elements as in the MIMO case. In our simulations and measurements for SA-SAR, one antenna is excited and the other one is terminated with a 50 ohm (Ω) load. When the antennas are highly coupled, the power fed to one port leaks to the other and the *E*-field distribution can be greatly changed, which will affect the SAR field distribution. Even though only one antenna is used at a time, there is minor hotspot obtained at the location of the other (unexcited) antenna, as seen in the SAR distribution field depicted on the right half in Fig. 3.

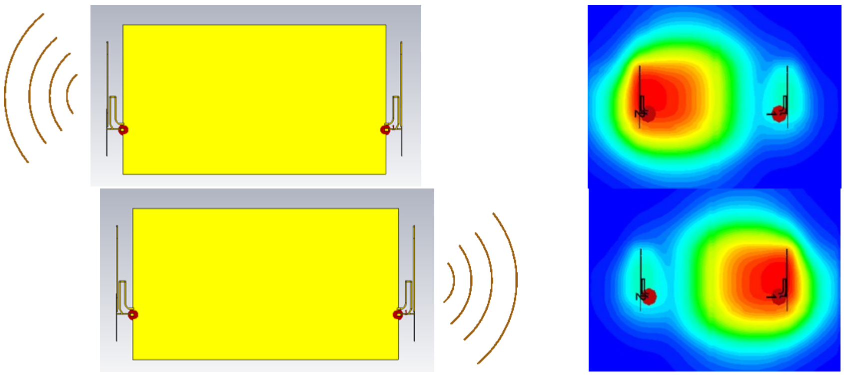

Figure 3: SA-SAR – excitation of single antennas vs. SAR distributions

2.3.2 Simultaneous SAR

Spatial Multiplexing (SM) is a MIMO technique that transmits independent and separately encoded data signals from each of the multiple antennas. Therefore, the space dimension is reused or multiplexed, increasing the capacity of the communication system. In the recently deployed LTE-Advanced standard, multiple antennas in the terminal are also simultaneously used in the uplink.

Another frequently used MIMO technique is adaptive beamforming, with which the Signal-to-Interference ratio (SINR) of the channel is increased by applying different weights through a coding matrix to the transceiver and changing the radiation pattern of the antenna system [6]. When the SINR increases, the quality of the communication link is improved. Different weights correspond to different phase differences exp($j\Delta\varphi$) between the antenna ports and this will produce different SAR values. An example of how the phase difference affects the far-field radiation pattern is given in Fig. 4 for the talking mode.

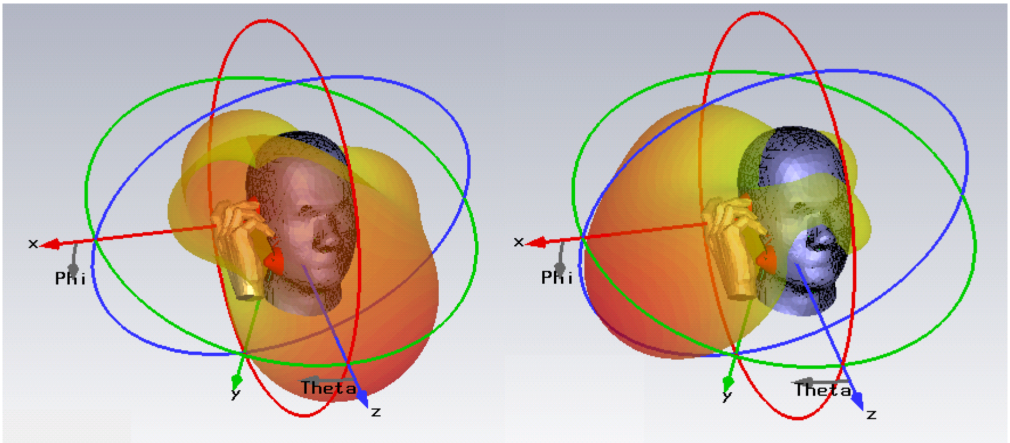

(a) $\Delta\varphi=90^{o}$ (b) $\Delta\varphi=270^{o}$

Figure 4 : Beamforming visual example in CST (talking mode): by changing the phase exp($j\varphi$) of the input signals the radiation properties change.

For the transmission schemes described above, multiple antennas are excited simultaneously. Hence SAR for both antennas has to be considered, which is defined in this work as Simultaneous SAR (or MIMO-SAR). MIMO-SAR is illustrated in Fig. 5.

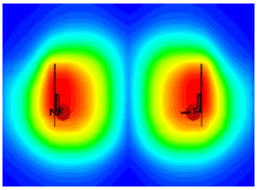

Figure 5: Simultaneous SAR – simultaneous excitation of both antennas at zero phase offset vs. SAR distributions

2.4 Methods for calculating MIMO SAR

2.4.1 SAR to Peak Location Spacing Ratio (SPLSR)

In [7], when two antenna elements are excited simultaneously, the method of SAR to Peak Location Spacing Ratio (SPLSR) is used as a concept to understand how closely located antennas can affect the final value of SAR. SPLSR is defined as:

$$SPLSR = \frac{SAR1+SAR2}{D} \quad [\mathrm{W/Kg/cm}] \qquad (2)$$

SAR1 and SAR2 are the SA-SAR values for each corresponding antenna element and *D*, which is the distance between the two SA-SAR hotspot peaks, is measured in cm (see Fig. 6). The FCC standard regulates that SPLSR should be less than 0.3 when the two antenna elements are spaced less than 5 cm from each other.

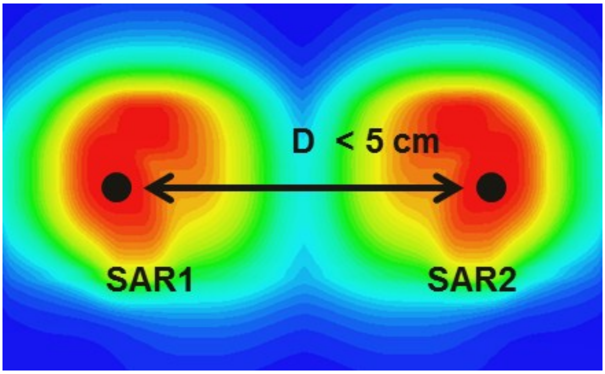

Figure 6 : Graphic Representation of SPLSR method

When the distance between the hotspots is less than 5 cm and the SPLSR is larger than 0.3, then MIMO SAR has to be further investigated, including simultaneous transmission with volume scans for both (or all) antenna elements. It should be noted that, SPLSR, which has a unit of [W/Kg/cm], is not a real SAR value. Instead, it is only a criterion to decide whether the simultaneous SAR needs to be further investigated or not. Thus, it is not fair to compare different antenna setups using SPLSR.

2.4.2 Average and Maximum MIMO SAR

In the previous section we have discussed that the phase difference between the signals across the ports is either due to the random signals from the two ports (in SM), or adaptive beamforming weights that change from time to time. Therefore, the phase difference can be considered as a uniformly distributed random variable. A straightforward metric that can give insight into the overall performance of MIMO-SAR is the averaged MIMO-SAR. In this case two ports are excited at the same time, with a phase shift between the ports varying over 0^o-360^o. MIMO SAR value is calculated for each phase shift and then averaged.

$$MIMO\text{-}SAR = \frac{\sigma}{2\rho}\left|\overrightarrow{E_1} + \overrightarrow{E_2}e^{-j\varphi}\right|^2 \quad [W/Kg], \quad \varphi \in [0,360] \qquad (3)$$

where $\overrightarrow{E_1}, \overrightarrow{E_2}$ represent the induced E-fields generated by each antenna and φ is the phase difference between the two ports.

The total E-Field produced by both ports will vary with phase difference. This forces the corresponding SAR to be different as well. In such way we can also acquire a SAR trend, where the maximum SAR value can be observed. Figure 7 shows an example of how a SAR trend is obtained when we evaluate the MIMO-SAR with (3).

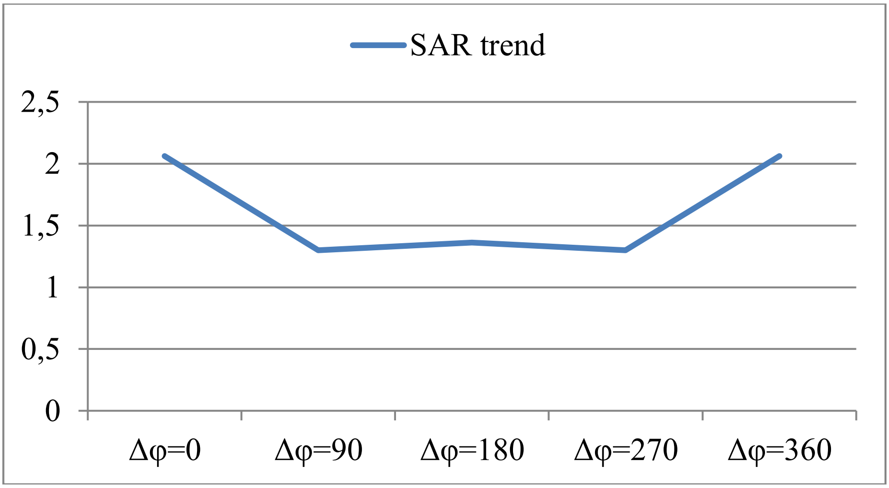

Figure 7 : MIMO-SAR graphical illustration

CHAPTER 3

3 Antenna Configurations

3.1 Mobile Antenna Designing Aspects

Inside a mobile handset the antennas are integrated in the small chassis and they become part of the mobile itself. From the fundamental design perspective, closely spaced antennas generate higher spatial correlation and mutual coupling, which in turn degrade the performance of MIMO systems when it comes to efficiency, bandwidth, diversity gain and capacity.

For practical considerations, when there is more than one antenna physically distributed within the compact terminal, the antenna radiation performance becomes more sensitive to user proximity. In particular, the head, hand and body, which are in the reactive near field of the mobile handset antennas, can significantly influence the antenna impedance, radiation patterns, efficiency and current coupling between antenna elements. Thus, the likelihood of one or more antennas being detuned by the hand or head of the user is increased, due to the allocation of more antennas in the terminal.

For frequencies lower than 1 GHz, the isolation of the antennas becomes more complicated because the wavelength is relatively large in comparison to the typical size of mobile terminals. For example, at 900 MHz, one wavelength is 0.333 m, which implies that multiple antenna elements in a 120 cm × 60 cm handset can at most be separated by about a third of a wavelength.

More importantly, in the low frequency bands, the mobile chassis becomes the main radiator, unlike the higher frequency bands where the chassis only functions as a ground plane. This is a critical aspect to consider when design a multiple antenna terminal [9]. The interaction between the antenna elements and the characteristic modes of the chassis are very important aspects to consider when designing multiple antennas in compact mobile terminals. Previous related work [9] has shown that when one electric antenna is located at a short edge of the chassis, the fundamental characteristic mode of the chassis is excited and the current is distributed over the whole chassis. In this thesis work, the selection of the antenna position, design and type is based on how the localization of the chassis current and the isolation of the antennas can affect the SAR values; and how this impact can reduce the radiation absorbed by the human body.

3.2 Frequency Specifications

The aim is to design antennas that work in both LTE B5 and B2 bands. Details for the specifications can be found in Table 2:

Table 2 : Frequency specifications

LTE B5 band	LTE B2 band
824–894 MHz (824–849 and 869–894)	1.850–1.990 MHz (1.850–1.910 and 1.930–1.990)
70 MHz bandwidth	140 MHz bandwidth

3.3 Mobile Multi-antenna Prototypes Overview

In this section a brief overview of the seven antenna setups will be presented along with the motivation behind why these dual-antenna setups are chosen to investigate MIMO SAR. For consistency, the dimensions of all the antennas are **130×66 mm**. The antenna setups are depicted in Fig. 8. In this thesis, we investigate three influential factors for SAR:

- *Antenna Locations*: When it comes to antenna location, we want to investigate how the same antennas located in different position can impact the SAR value. For prototype B we use two identical couple-fed monopoles on the same short edge of the chassis, whereas in B2 the identical monopoles are placed on the opposite edges. In addition, prototypes A, B2, E and F have identical antennas in similar locations.
- *Antenna Types*: Prototypes C, E and F are compared to give insight on how the type of antenna can change the SAR value. Prototype C consists of a Planar Inverted-F Antenna (PIFA) on one edge and a monopole antenna on the other edge of the chassis. Prototype E has two identical monopoles on the two edges, whereas prototype F has two identical PIFAs.
- *Different Chassis Excitation Level*: Both antennas in Prototype A excite the fundamental characteristic mode of the chassis, since the monopole antennas are placed on the short edges. In Prototype D, the T-strip antenna located along the long edges utilizes a mode orthogonal to the monopole. This makes the radiation patterns of the

two antennas orthogonal and it is expected to produce interesting results for MIMO SAR.

CST Microwave Studio is used to perform full wave electromagnetic simulations for the antenna structures. Properties such as S-parameters and radiation pattern will be presented for each prototype in the next chapter.

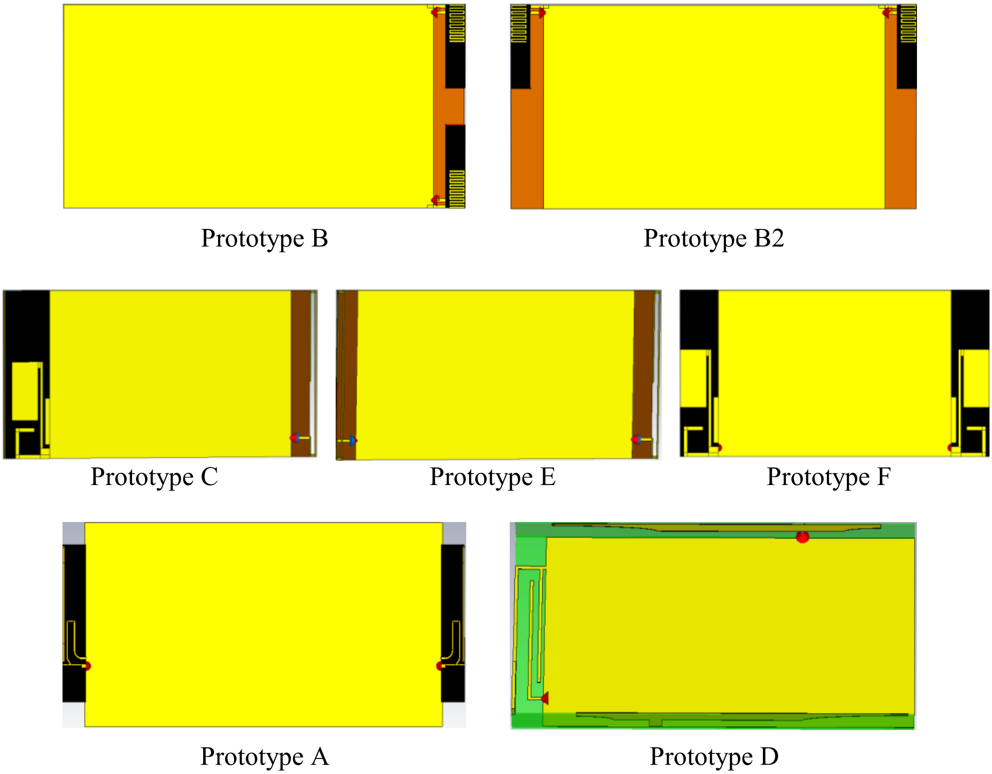

Figure 8 : Prototypes overview

CHAPTER 4

4 Antenna Prototypes

In this chapter, the prototypes used in the thesis work are presented in detail.

4.1 *Prototype A: Dual Monopoles on Two Edges of the Chassis*

4.1.1 Antenna Design

Prototype A (PA) consists of two identical dual-band inverted-F antennas (IFAs) located on the short edges of the chassis. IFAs are commonly used in mobile phones, due to their simplicity and good performance.

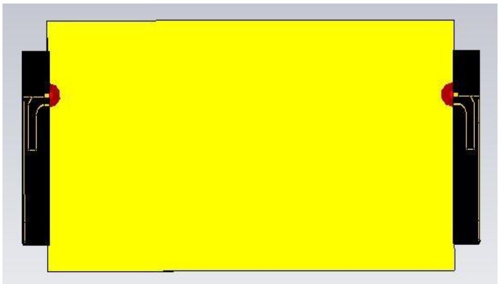

(a) Simulated handset design in CST

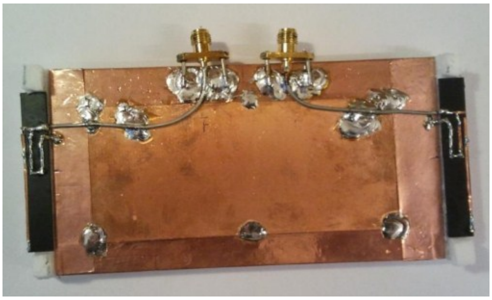

(b) Fabricated prototype

Figure 9 : Prototype A

4.1.2 Antenna Characteristics

The shape and dimensions of the antenna are optimized to achieve the desired band coverage. The simulated and measured S parameters are shown in Fig. 10, where the desired bands are covered. For clarity, the center frequency of each band is noted in the plots.

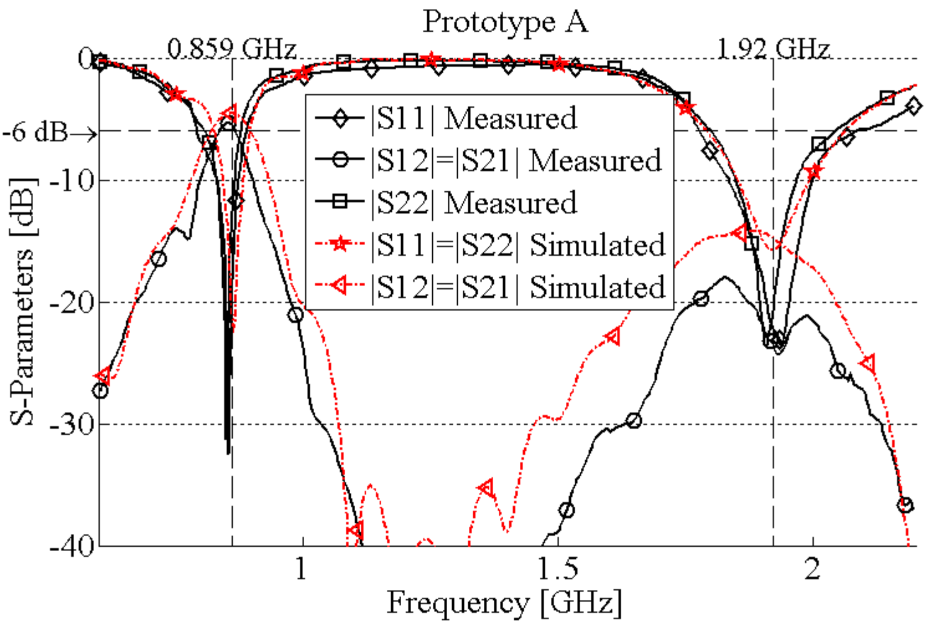

Figure 10 : Magnitude of the reflection and coupling coefficients (S Parameters) for the two ports in dB of Prototype A.

It is known that when the antenna elements are placed at the two short edges of the chassis, they excite the same characteristic mode. In this mobile configuration, the monopoles are located in the opposite chassis edges and excite the entire chassis to radiate like a flat electric dipole. Both antennas share the chassis as their radiator and that causes high mutual coupling of around -6 dB [9], [11].

4.2 Prototype B: Dual Co-Located Coupled-Fed Monopoles

4.2.1 Antenna Design

To compare the influence of different antenna locations, two coupled fed monopoles are placed symmetrically on the same short edge of the chassis (Prototype B – PB, as seen in Fig. 11). The antenna itself is a dual band monopole, consisting of a feeding element along with a parasitic element that extends from the ground plane to create a dual band excitation.

The dual elements are placed at the bottom side of the handset in order to provide lower SAR values in the “talking mode”.

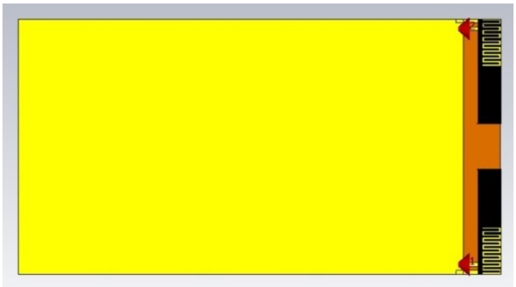

(a) Simulated handset design in CST

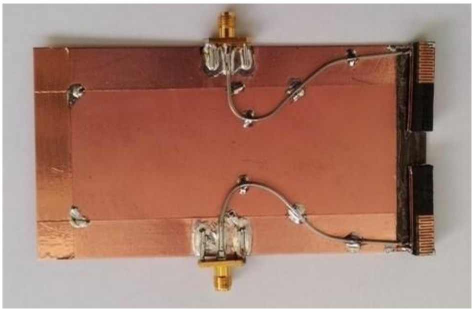

(b) Fabricated prototype

Figure 11 : Prototype B

4.2.2 Antenna Characteristics

The shape and dimensions of the antenna are optimized to achieve the desired band characteristics. The bandwidth of PB is quite large, especially in the higher band.

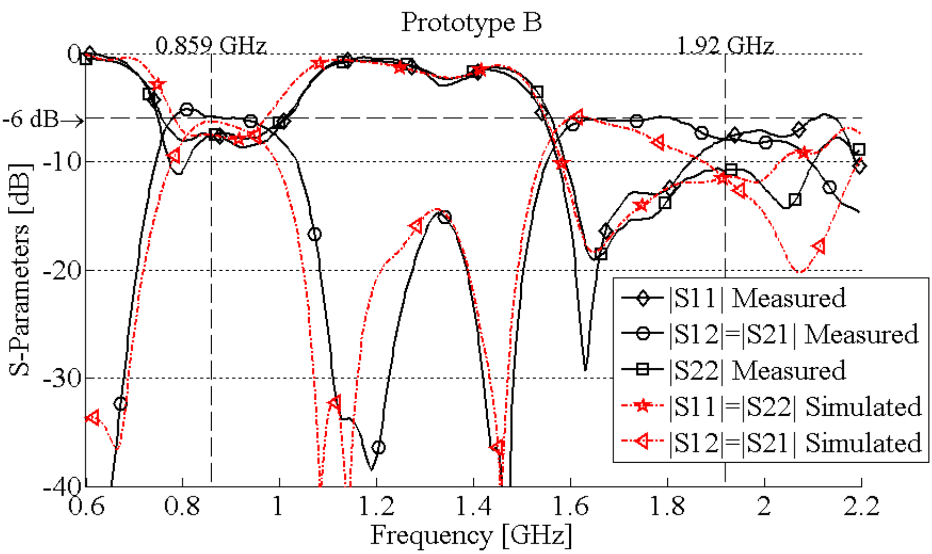

Figure 12 : Magnitude of the reflection and coupling coefficients (S Parameters) for the two ports in dB of Prototype B

The S-parameters for PB are shown in Fig. 12. High coupling (almost -6 dB) is also observed in the low frequency band, similar as for PA, which is because the chassis is acting as a shared radiator and the current leaks from one port to the other.

4.3 Prototype C: On-Ground PIFA and Monopole

4.3.1 Antenna Design

The third handset (Prototype C – PC) utilizes a PIFA at the top edge and a monopole at the bottom side (see Fig. 13). The PIFA (port 1) is an on-ground PIFA, meaning that the chassis extends under the entire planar antenna element (equivalently, there is zero clearance for the antenna along the plane of the chassis), as opposed to other designs such as semi ground free or ground free antennas (as defined in [13]). The on-ground design influences the SAR value with respect to the orientation of the antenna. The shorted parasitic branches are used for the high frequency band operation [12]. A folded monopole antenna (port 2) is utilized on the other short edge of the chassis.

(a) Simulated handset design in CST

(b) Fabricated prototype

Figure 13 : Prototype C

4.3.2 Antenna Characteristics

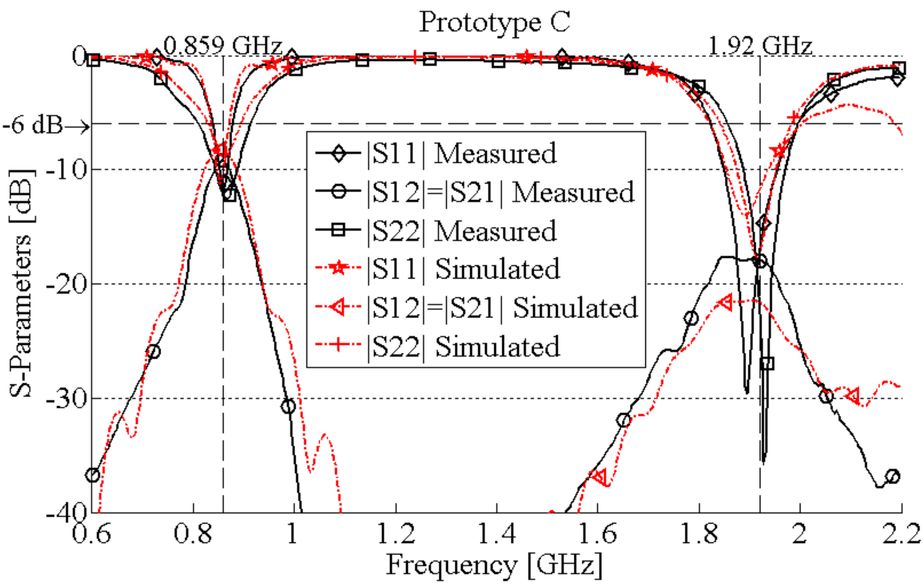

Figure 14 : Magnitude of the reflection and coupling coefficients (S Parameters) for the two ports in dB of Prototype C

It is observed from Fig. 14, that the PIFA does not exactly meet the -6dB criterion in the entire frequency bands of interest. This is due to its inherent narrow band characteristics. Compared with monopole antennas, the bandwidth of PIFAs is narrower and the current on PIFAs is more localized [9]. Usually, PIFAs are used as diversity antennas. The monopole placed in the bottom of the chassis has larger bandwidth and can be considered as the main antenna. For PC, the isolation in the low band is higher (9 dB) due to the more localized current of PIFA.

4.4 Prototype D: T-Shaped Strip Antenna and Monopole

4.4.1 Antenna Design

In Prototype D (PD) (Fig. 15), two T-strips are vertically connected to the longer edges of the chassis (port 1) and a broadband monopole is used at one short edge of the chassis (port 2). The T-Strip antenna has slightly modified the chassis to allow it to operate in two orthogonal modes. This prototype is based on the recent work of [13], and it can give insight into how SAR values are affected when orthogonal chassis modes are excited by different antennas. The monopole easily excites the chassis since it is an electric antenna and exhibits strong currents along the length of the chassis. The T-shaped antenna on the long edges focuses the current on the two metal strips and they operate as a capacitively loaded dipole along the width of the chassis. The two antenna types excite different characteristic modes and generate orthogonal radiation patterns and low mutual coupling.

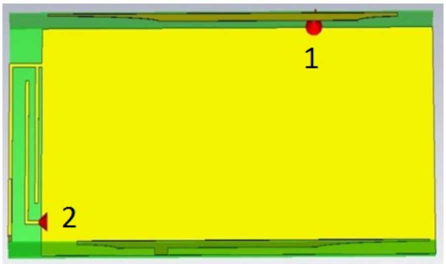

(a) Simulated handset design in CST

(b) Fabricated prototype

Figure 15 : Prototype D

4.4.2 Antenna Characteristics

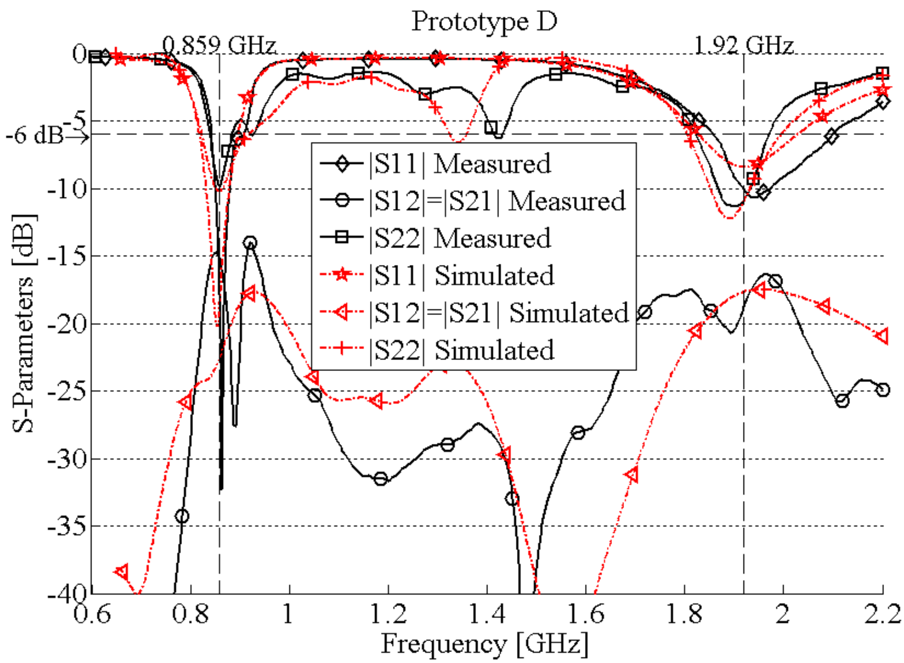

Figure 16 : Magnitude of the reflection and coupling coefficients (S-Parameters) for the two ports in dB of Prototype D

We mentioned in the previous chapter that for frequencies below 1 GHz, it is challenging to achieve low mutual coupling in mobile handsets. However, due to the orthogonal modes excited, PD can obtain high port isolation in both the low and high frequency bands, as shown in Fig.16. Also, both the T-Strip antenna and the monopole antenna provide good bandwidth for the two operating bands.

4.5 Prototypes B2, E and F: Identical antennas at the opposite edges of the chassis

To facilitate interesting comparisons with some of the previous prototypes, prototypes with identical antennas at the opposite short edges of the chassis are generated. Prototype B2 (PB2) is designed for comparison with PB whereas both Prototype E (PE) and F (PF) are designed for comparison with PC. Specifically:

- PB2 has the same monopole antenna as PB. The SAR properties of this prototype will be compared with PB since we want to investigate how different antenna locations can affect SAR when the same antennas are used.
- PE consists of two identical folded monopole antennas at the short edges and can be considered as the prototype most similar to PA. The antennas utilized in this handset are the same as the monopole used for port 2 of PC.
- PF is designed with two identical PIFAs at the opposite short edges of the ground plane. The antennas are the same as the PIFA used for port 1 of PC.

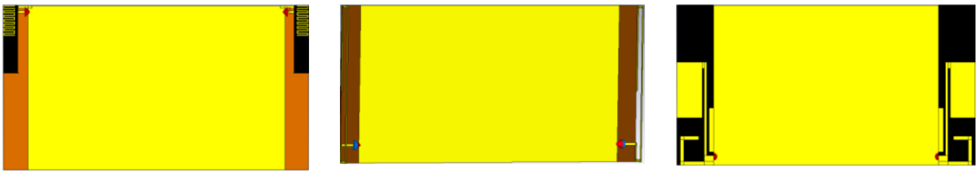

Prototype B2 Prototype E Prototype F

Figure 17 : Prototypes with identical antennas at the opposite short edges

CHAPTER 5

5 CST Simulations Setup

5.1 CST

CST Microwave Studio has been approved by FCC to comply with the FCC SAR standard and is widely used for SAR simulations. Finite-Difference Time-Domain (FDTD) is a well-known time domain simulation method that directly discretizes the partial differential form of Maxwell's equations. Time domain solver implementation in CST is based on the Finite Integral Time-Domain (FITD) method and outperforms FDTD by orders of magnitude both in speed and accuracy [15]. CST offers the whole body averaged and local SAR values. Local SAR is given as a numerical value per volume element and becomes a space distribution function. It is averaged in tissue masses of 1 g as defined by ANSI/IEEE C95.1-1992 of the United States, where a cuboid averaging volume is used.

5.2 Reference Power, Target Frequencies and Handset's Side definitions

The default input power in CST is 1 W peak power. The results of SAR values can be rescaled by setting a user defined power since the SAR value varies linearly with the accepted power. In this study, the accepted powers to the antennas for the SA-SAR case are set to **24 dBm (0.25 W)** for the low band (824-894 MHz) and **21 dBm (0.13 W)** for the high band (1850-1990 MHz) [14]. The accepted power is used to represent the worst case SAR, since the antenna mismatch, which can reduce the radiated power and the SAR value, is excluded. The other reason for utilizing accepted power is that antennas will be detuned differently when they are in proximity of the flat phantom. For MIMO-SAR we **divide the power equally** in both antennas so the total power fed in both elements is equal to the maximum accepted power for each band. In the simulations and measurement campaign the target frequency is the **center frequency of each band,** i.e., 859 MHz and 1.92 GHz for the LTE B5 and B2 bands respectively. The setups of the power and frequencies are summarized in Table 3.

Table 3 : Power and Frequency Specifications

Operating Band	LTE B5	LTE B2
Frequency Range	824 – 894 MHz	1850 –1990 MHz
Center Frequency	859 MHz	1920 MHz
Accepted Power	24dBm (0.25W)	21dBm (0.13W)

Different placement sides of the prototypes are also studied. Side 1 means the chassis side is close to the phantom, which corresponds to the case where the screen is facing the user's body. Side 2 refers to the case where the antennas (back side or battery side of the mobile) are close to the phantom.

CHAPTER 6

6 Simulations with Flat Phantom (Body Worn Mode)

6.1 Flat Phantom Model

Body worn mode refers to the case where the user keeps the mobile in the pocket. A flat phantom is used to simulate the human body. It is composed of two layers: the inner liquid with the size of **225×150×150 mm^3** and an outer shell with thickness of **2 mm**. As long as the device is at a small distance to the flat phantom and the projection of the device is enclosed within the flat phantom surface with a distance to the edge of greater than 20 mm (see Fig. 18), the difference in SAR for any phantom of any shape and size is negligible.

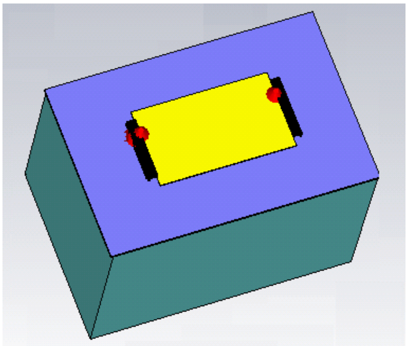

Figure 18 : The flat phantom mannequin in CST

In the simulation, we use the specific dielectric properties for the head and body at each frequency of interest, as defined by FCC [16]. This makes the simulation faster and the results accurate. The properties of the inner liquid and the outer shell at the frequencies of interest are listed in Table 4. In our study, each prototype is placed **3 mm** above the phantom regardless of the sides, as illustrated in Fig. 19, and the distance is defined between the flat phantom and the element (antenna or chassis) that is closest to the phantom (Fig. 19).

Table 4 : Dielectric properties of flat phantom liquid

	Target Frequency [MHz]	Relative Permittivity ε_r	Conductivity σ [S/m]
Inner liquid	859	41.5	0.926
	1920	40	1.4
Outer shell	859 & 1920	3.7	0.0016

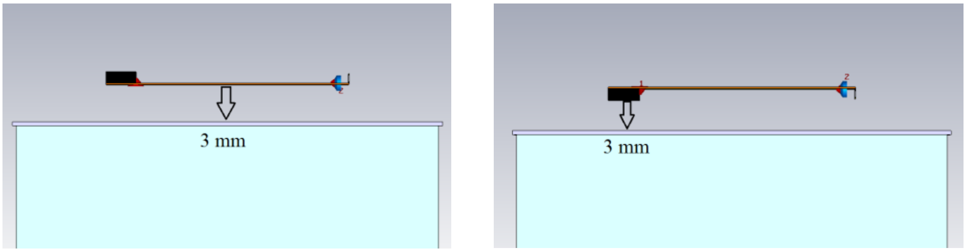

(a) Prototype C side 1 (b) Prototype C side 2

Figure 19: Distance and positioning for the flat phantom set-up (example for PC)

6.2 *Influence of the Antenna Location*

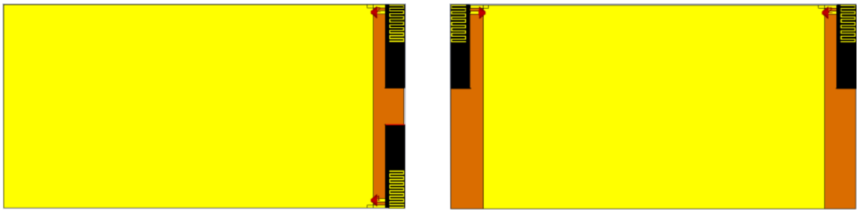

Prototype B Prototype B2

Figure 20 : Prototypes B and B2, studied for the influence of the antenna location on SAR

6.2.1 Stand-Alone SAR

To begin with, we study the SA-SAR first in this section, where only one antenna is excited. The SA-SAR can help us to investigate how the different antennas behave while operating separately and later a more comprehensive comparison with dual port excitation will be carried out. The simulation results for SA-SAR on the flat phantom are presented in Fig. 21 for PB and PB2. Since the two antennas in each setup are identical to each other and placed in mirror symmetry on the prototype, the results are identical for both antennas, and hence shown for only one port.

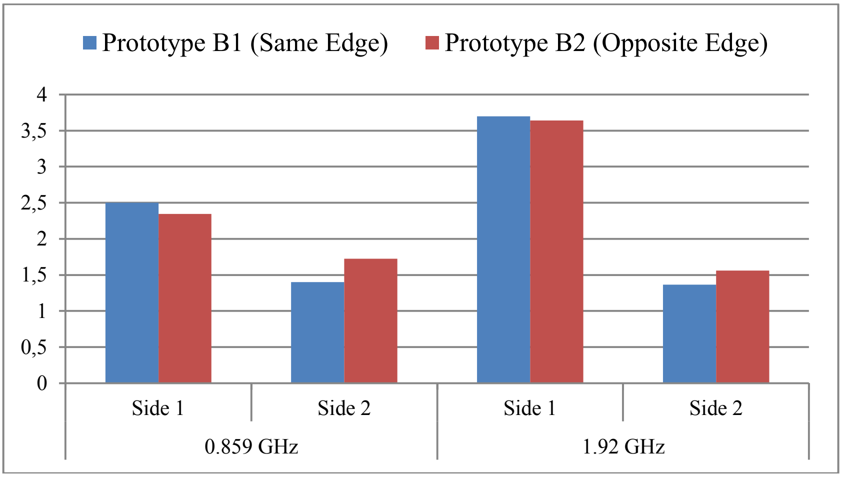

Figure 21: SA-SAR for Prototypes B and B2

It is observed that the co-located and separated antenna setups provide similar SA-SAR values, even though the separation distance between the antennas differs significantly for the two cases. When the coupled monopole is placed at a short edge of the chassis, the chassis is excited as an efficiency radiator, which radiates as a dipole along the chassis length [9]. The simultaneous excitation of the chassis by both antennas induces similar radiation behavior, such as mutual coupling, current distribution and *E*-field distribution for the two setups. For this reason, the SAR values and distributions are almost identical.

The observation above can be well explained if we check the magnitudes of the *E*-field. At a plane 12 mm below the chassis for both setups at 0.859 GHz *in free space*, the *E*-field is presented in Fig. 22, with the solid black frame indicating the position of the mobile handsets. It is seen that the *E*-field distributions show similarity with each other even though the antenna locations differ a lot. Furthermore, the *E*-field distributions are similar as that for a flat dipole along the chassis length. Since SAR is directly related to the *E*-field according to (1), it is expected that the SAR values for both setups are similar.

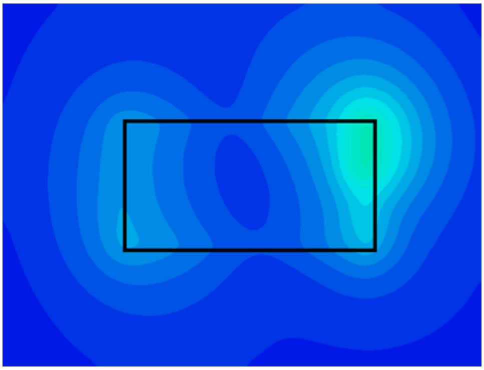

(a) Co-located antennas (PB)

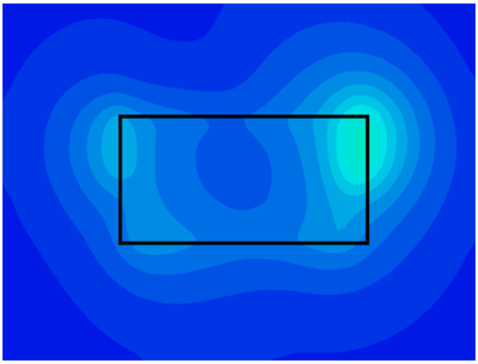

(b) Antennas at the opposite edges (PB2)

Figure 22 : Magnitude of *E*-field distributions for different antenna setups in free space at 0.859 GHz

PB-S1			
859 MHz		1.92 GHz	
Port 1	Port 2	Port 1	Port 2
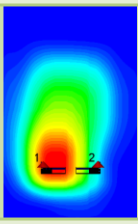	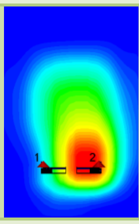	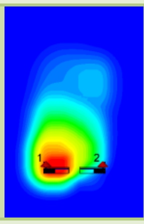	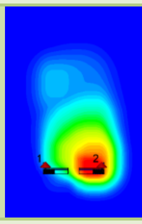
2.575 W/Kg	2.575 W/Kg	3.7 W/Kg	3.7 W/Kg
PB2-S1			
859 MHz		1.92 GHz	
Port 1	Port 2	Port 1	Port 2
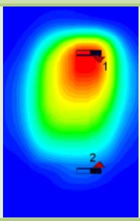	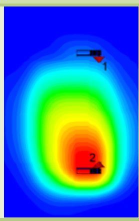	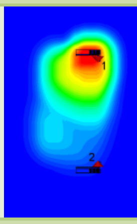	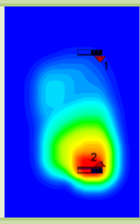
2.33 W/Kg	2.33 W/Kg	3.64 W/Kg	3.64 W/Kg

Figure 23: SA-SAR field distributions for PB and PB2 (Side 1)

Figure 23 shows the SA-SAR fields for PB-Side 1(S1) and PB2-S1, where the SAR distribution in each case is normalized to the maximum peak SAR. It is observed that the SAR distributions are similar for the two setups. However, if considering different sides (SAR distributions for Side 2 are shown in Appendix A1), it is found that S1 gives almost twice as high SAR values as S2. This is because the chassis works as an effective radiator, and it is closer to the phantom at S1 than at S2. At the high frequency band, a second small hotspot is observed, since the higher order mode of the chassis (full wavelength dipole mode) is excited at this frequency band. This can be more clearly observed in the SAR distribution for Side 2, which is shown in Appendix A1.

6.2.2 MIMO-SAR

The simulations of the MIMO-SAR follow the procedure in Section 2.4.2. The two ports for each prototype were excited simultaneously and we applied the phase sweep principle as discussed in (3) for averaging. Figure 24 illustrates the average MIMO-SAR distributions over different phase shifts between the signals in the ports. It is observed that when the absorption is more spread under the chassis, SAR is lower; whereas the value is higher when the focused hotspot is located below the antenna elements.

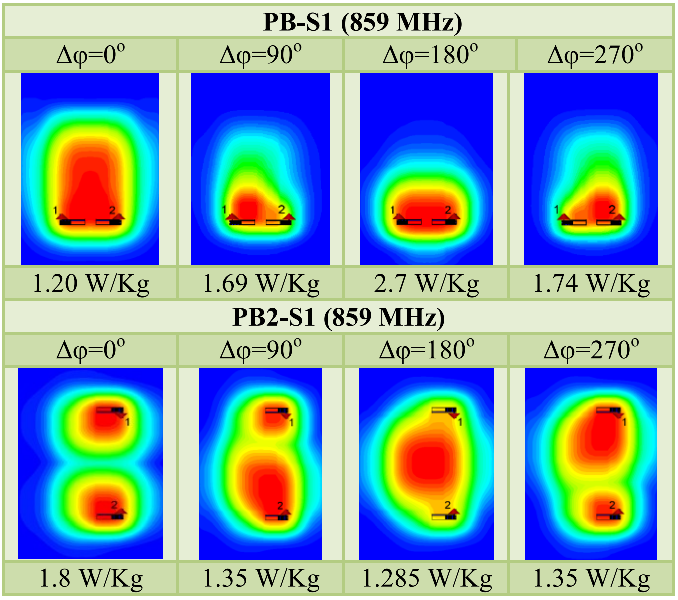

Figure 24: MIMO-SAR distributions for PB and PB2 at 0.859 GHz

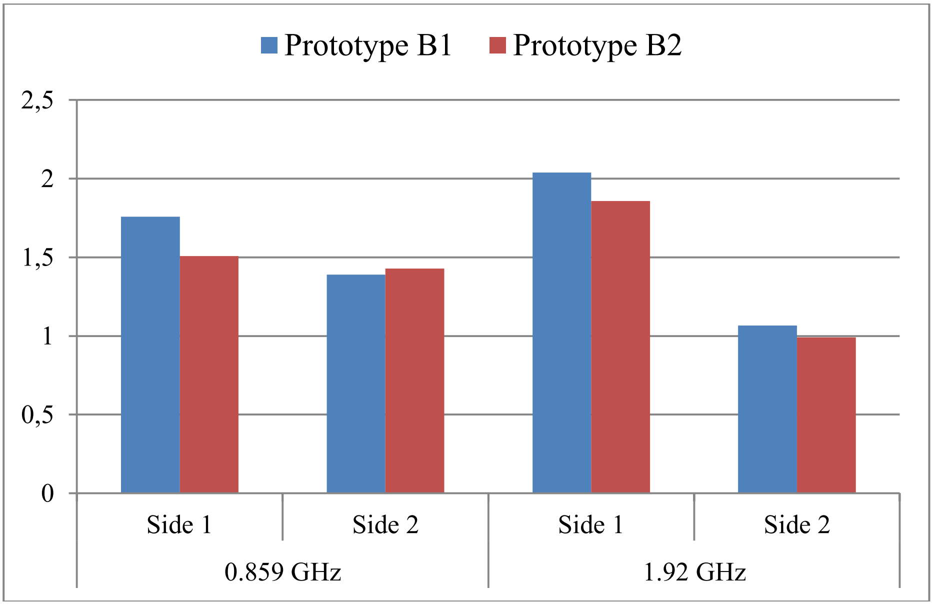

Figure 25: Average MIMO SAR for Prototypes B and B2

Although the SAR distributions for PB and PB2 are different, the averaged MIMO-SAR is similar, as shown in Fig. 25. The comparison between average and maximum MIMO-SAR values for all prototypes can be found in Appendix A2.

Together with the SA-SAR results, it is indicated that the SAR values are similar for the co-located and separated monopole setups. In practice, using the co-located monopoles as in PB has the advantage of saving precious space for other components in the mobile terminal. Moreover in the talking mode, it can provide a lower SAR value due to the larger distance between the antennas and the chin, as will be shown in Chapter 8.

6.2.3 SAR to Peak Location Spacing Ratio Method

The definition and requirements of SPLSR has been defined in Section 2.4.1 as:

$$SPLSR = \frac{SAR1 + SAR2}{D} < 0.3 \quad when \quad D < 5cm$$

The method defines the distance *D* between the two hotspots for SA-SAR. When the separation distance between the two hotspots is less than 5 cm, and the SPLSR is larger than 0.3, the antenna pair should be included in the simultaneous transmission testing, since the SAR peak can be higher than the requirements. In this section, we will study the SPLSR for Prototype B – Side 1 at low frequency band (PB-S1-L).

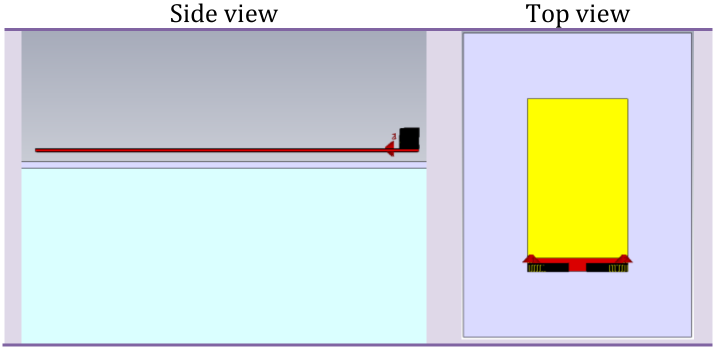

Figure 26: Evaluating SPLSR for D < 5 cm, we use PB for: Side 1, 0.859 GHz (PB-S1-L)

Figure 27 depicts the SAR distribution levels with respect to the position on the flat phantom (along the short edge): For the prototype of PB-S1-L, when port 1 is excited, then the impact of the absorption levels can be visualized as the green grid in the figure. Accordingly for a separate excitation in port 2 the blue grid is obtained. The two distributions are plotted together in the same graph and we observe that the distance between the hotspots is 3.26 cm, which fulfills the SPLSR criterion of D < 5 cm. The SPLSR is calculated as:

$$SPLSR = \frac{SASARP1 + SASARP2}{D} = \frac{2.75 + 2.75}{3.26} = 1.57$$

When the prototype is operating in SM scheme and simultaneous SAR is studied, then the results in Appendix A2 are observed. In this case, the MIMO-SAR value through the phase sweep is minimum at $\Delta\varphi=0^{o}$ and this is represented by the red grid in Fig. 27. The maximum MIMO-SAR occurs at $\Delta\varphi=180^{o}$, when the hotspots are located below the antenna elements (black grid). The yellow grid can be seen as an upper bound for the absorption level and it represents the addition of the green and blue grid (SA-SAR for P1 and P2). It is observed that the maximum MIMO-SAR for

Δφ=180° (black grid) only slightly excels the SA-SAR peaks (green and blue grids). This indicates that SPLSR method can lead a wrong expectation of SAR because the value that is obtained from the calculation is much larger than the limit (0.3). Therefore, SPLSR should only be treated as an indicator on whether to include simultaneous transmission measurements for all antennas or not, as originally intended for the metric.

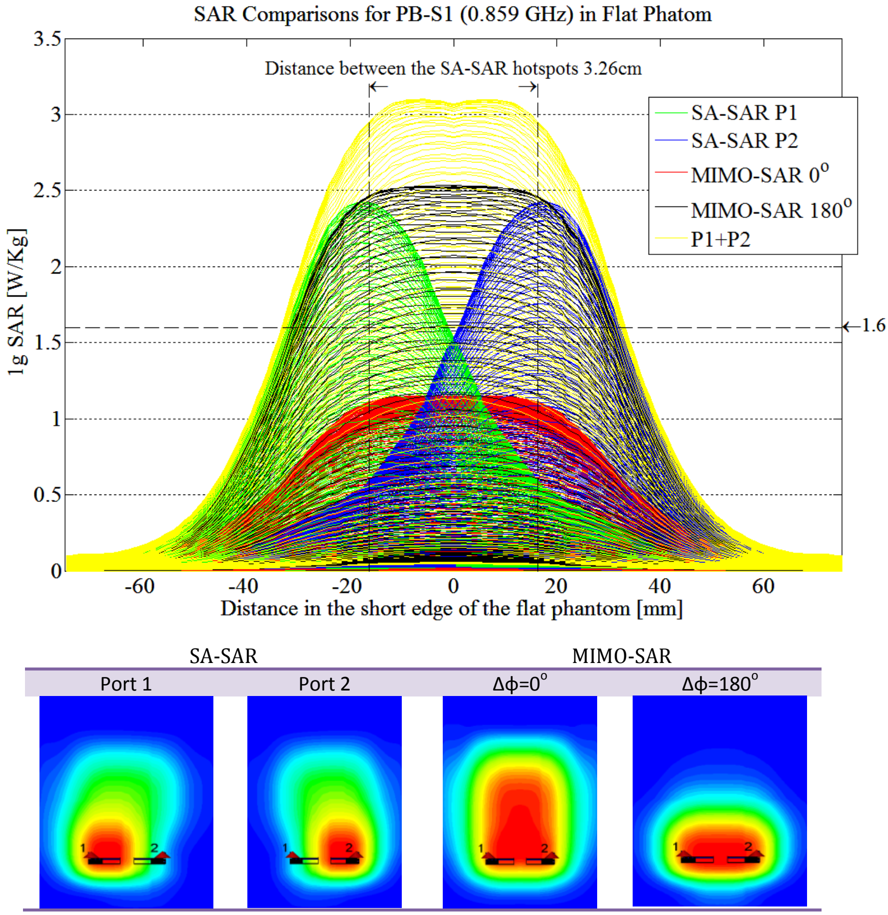

Figure 27: PB-S1-L SAR field distributions inside the flat phantom

An example on the application of SPLSR, that examines the case where D > 5 cm can be found in Appendix A2.

6.2.4 Identical Antennas at the Opposite Short Edges

We have seen that for PB2, where the antennas are located at the opposite edges of the chassis, SAR reaches its minimum value when the hotspot is well spread below the chassis, at $\Delta\varphi=180^o$. The simulations for PA (Fig. 28) which correspond to the same locations of antennas, give similar MIMO-SAR trend in the low band. This prompted us to further investigate and compare the MIMO-SAR behavior for prototypes A, B2, E and F, in which dual identical antennas are located at the opposite short edges of the chassis.

PA-S1			
859 MHz		1.92 GHz	
$\Delta\varphi=0^o$	$\Delta\varphi=180^o$	$\Delta\varphi=0^o$	$\Delta\varphi=180^o$
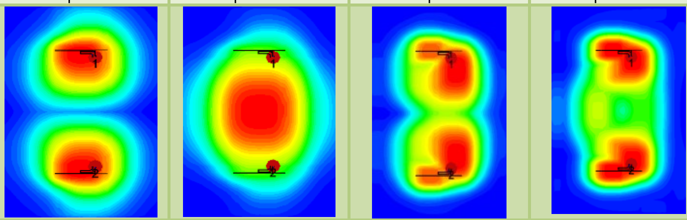			
2.06 W/Kg	1.36 W/Kg	1.03 W/Kg	1.20 W/Kg

Figure 28: MIMO-SAR field for Prototype A – Side 1

It has been mentioned earlier that the current distribution and thus the MIMO-SAR behavior change with the frequency bands. For the low frequency the fundamental dipole mode of the chassis is excited, and the current is higher across the ground plane. The SAR value then reaches the minimum point when the hotspot is located below the chassis, at $\Delta\varphi=180^o$ (see Fig. 28).

Figure 29 shows the difference in the MIMO-SAR trend when it comes to different sides. In S1, the SAR behavior is more stable, since the chassis is closer to the phantom and the current on the chassis is more spread. For S2, the antennas are closer to the human tissue and the SAR value is more determined by the current on the antenna elements and its induced *E*-Field. Thus, SAR varies more significantly as the phase shift is swept from 0^o to 360^o for this side.

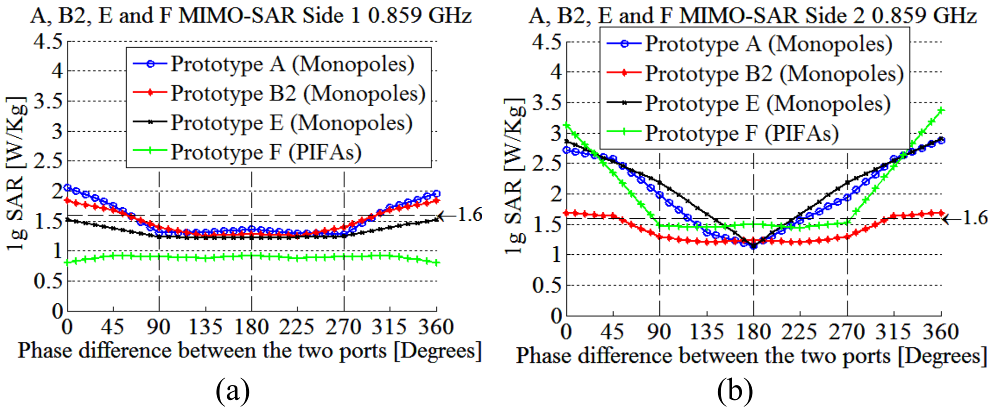

Figure 29: Comparison of MIMO-SAR for Prototypes A, B2, E and F at 0.859 GHz in both sides

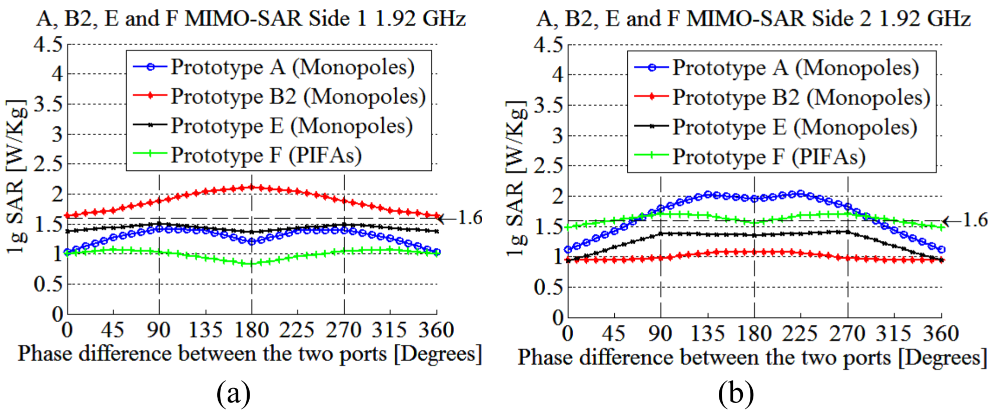

Figure 30: Comparison of MIMO-SAR for Prototypes A, B2, E and F at 1.92 GHz in both sides

For S1 at 1.92 GHz, PA, PE and PF give the maximum MIMO-SAR value when the phase shifts are 90° and 270°. PB2 is an exception, with its peak SAR value at 180°. These observations can be a subject of further investigation and can save time in measuring MIMO-SAR.

6.3 Influence of the Antenna Type

The antenna type plays an important role in SAR, since the current distributions can vary substantially for different antennas. PIFAs in general create a more localized current distribution, whereas the current for the monopoles is more evenly spread over the chassis. In this section we compare PC that consists of two different antenna types (PIFA-Port1 and Monopole-Port2) with PE (dual monopoles) and PF (dual PIFAs), where identical antennas of the same type as in PC are used. For clarity, the configurations of PC, PE and PF are shown in Fig. 35.

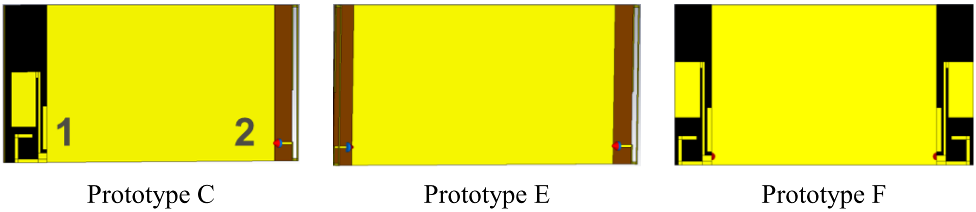

Figure 31: Prototypes C, E and F are studied for the influence of the antenna type on SAR

6.3.1 Stand-Alone SAR

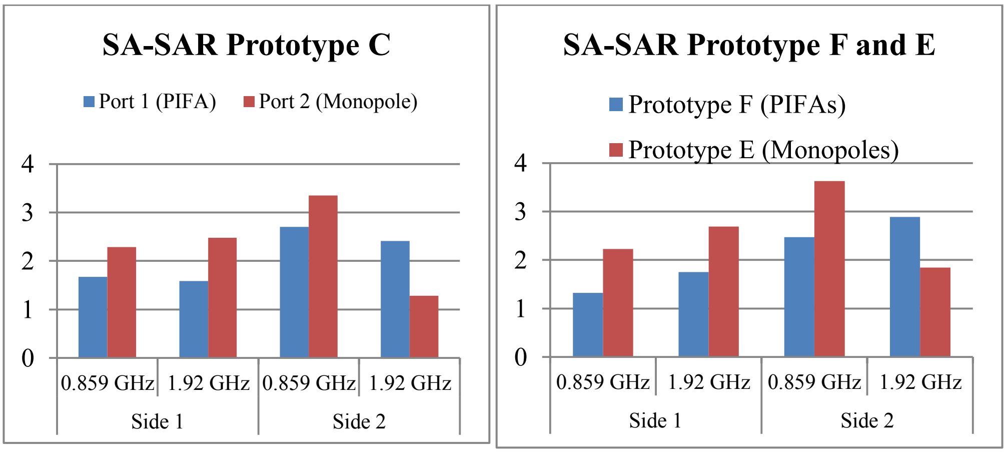

Figure 32: Stand Alone SAR values for different antenna types

In general for SA-SAR, it is observed that PIFA provides a lower SAR value compared with monopole except for S2 at 1.92 GHz. This exception is due to the current distribution along the antennas, which becomes significant when the antenna elements are facing the phantom. The magnitude of current distributions for monopole and PIFA are shown in Fig. 33.

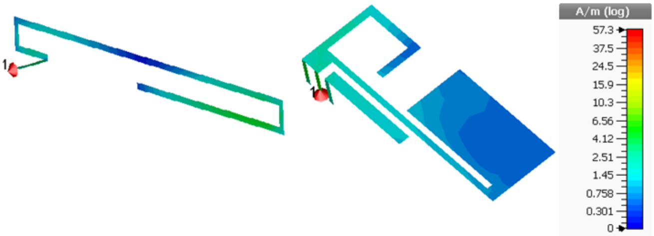

Figure 33: Current distribution for monopole antenna and PIFA at 1.92 GHz

It is noticed that for the monopole, the current at 1.92 GHz is stronger at its lower branch, which is close to the chassis. For the PIFA, the current is focused on the shorter branch on the patch. Accordingly, when the antennas are facing down to the flat phantom, the radiation source (current) for PIFA is closer to the phantom than the monopole, resulting in a higher SAR value. Since the PIFA provides a lower SAR value in general, if monopole and PIFA are used together in the mobile handset it is better to implement PIFA at the top and monopole at the bottom, to reduce the overall SAR value in the talking mode.

If different sides are compared, it is seen that S1 performs better than S2 in general. At S1, the current is spread along the chassis, which leads to a less-focused hot spot, and lower SAR values. On the contrary, the currents on the antenna elements play a significant role at S2, resulting in focused hot spots and higher SAR values. The exception of the monopole at 1.92 GHz is also due to its current along the lower folded branch.

6.3.2 MIMO-SAR

The simultaneous SAR for the three prototypes is shown in Fig. 34. Compared with the stand-alone SAR, the behaviors are similar, though MIMO-SAR has slightly lower SAR values in each case. If specific SAR values over different phase shifts are considered, for S1 (see Fig. 35), each SAR value is close to the average value, whereas for S2 (see Fig. 36) the difference between the minimum and maximum SAR value is larger. This is also because the chassis gives a more evenly spread distribution, compared with the focused distribution provided by the antenna elements when facing the flat phantom (Fig. 35).

For S1, the chassis is closer to the phantom and in the low band, the currents along the chassis are overall stable when the phase between the two ports changes. The induced *E*-Field inside the body does not change significantly in this case and so the MIMO-SAR value does not deviating a lot from the average. Particularly for PF, the SAR value is almost constant for any Δφ.

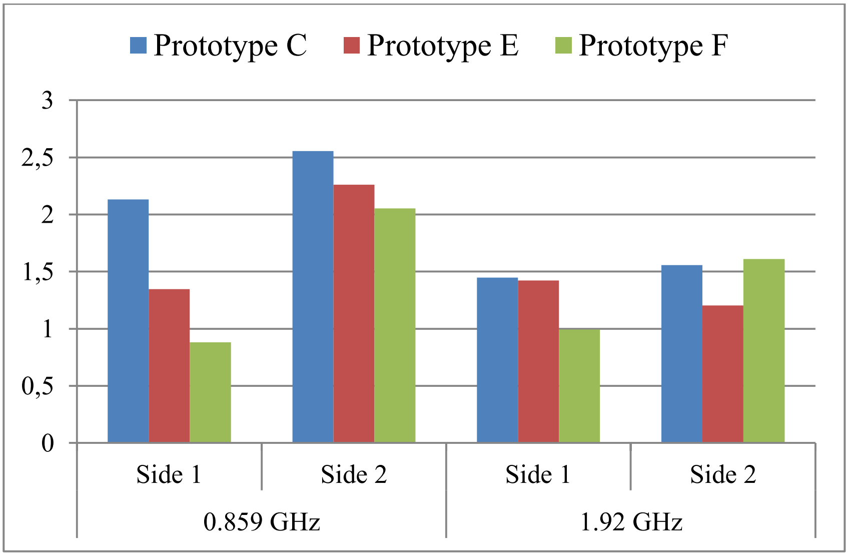

Figure 34: Average MIMO SAR for Prototypes C, E, and F

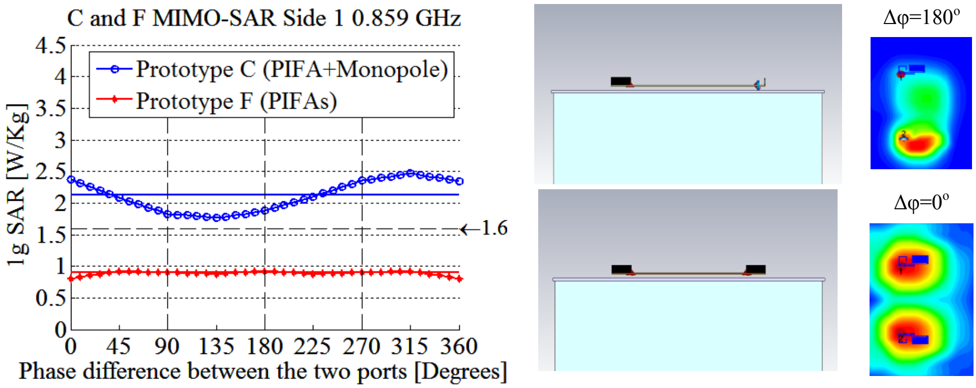

Figure 35: MIMO-SAR for Prototypes C and F at 0.859GHz (Side 1)

When the prototypes are at S2, the SAR values and distributions are shown in Fig. 36. It is observed that the SAR value for the PIFA varies a lot with the phase shift, and it generates a more localized hotspot. The current in this case runs across the vicinity of the PIFA and the antenna itself plays a more important role while it is closer to the phantom. It is also noted that the peak SAR occurs at 180° for PC whereas it occurs at 0° for PF.

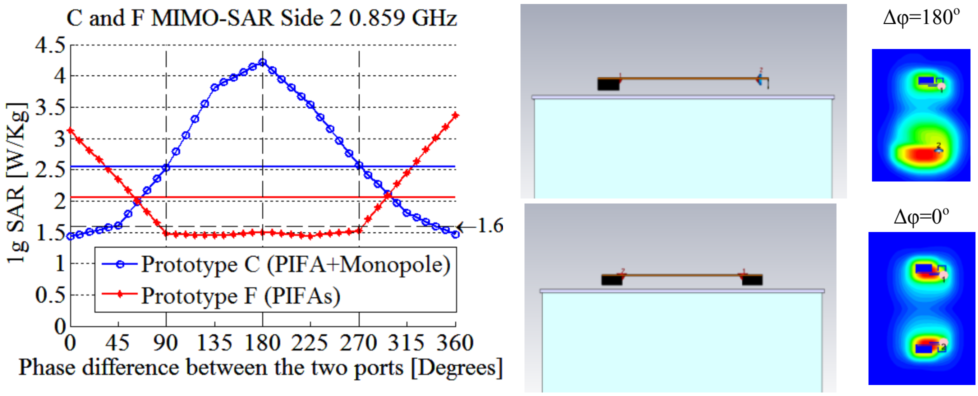

Figure 36: MIMO-SAR for Prototypes C and F at 0.859GHz

Moreover, at S2 the PIFA radiates towards the flat phantom and makes a significant impact on the total SAR value. For the low frequency band, at Δφ=0°, the current is well spread over the chassis, leading to a lower SAR value, while at Δφ=180° the *E*-field contribution from the PIFA adds constructively with that of the monopole to create a localized hotspot away from the center. This gives a much higher SAR value. At 1.92 GHz the SAR value is mainly determined by the PIFA (see Fig. 37).

PC-S2			
859 MHz		1.92 GHz	
Δφ=0°	Δφ=180°	Δφ=0°	Δφ=180°
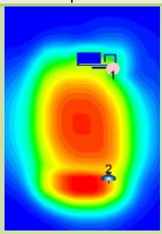	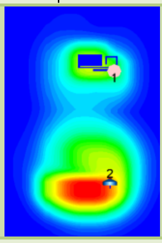	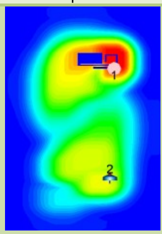	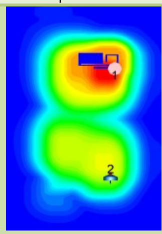
1.42 W/Kg	4.22 W/Kg	1.72 W/Kg	1.57 W/Kg

Figure 37: MIMO-SAR Distribution for Prototype C

6.4 Influence of the Chassis Excitation

In this section, Prototypes A and D are utilized to study the influence of different chassis excitation levels.

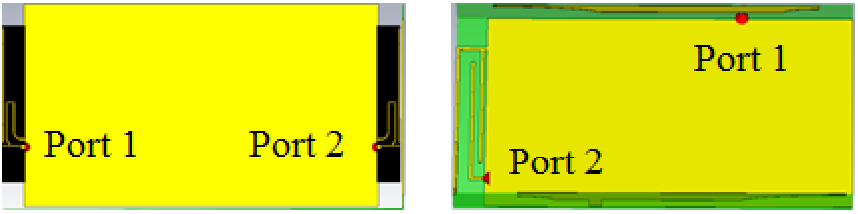

Prototype A   Prototype D

Figure 38: Prototypes A and D studied for the influence of the chassis excitation on SAR

In the introduction we mentioned that for most of mobile terminals at frequencies below 1 GHz, the chassis radiates as part of the antenna, leading to high mutual coupling when it comes to multiple antenna elements attached to it. As a new antenna design method, PD was proposed in [13], where a T-strip antenna fed along the long edge of the chassis is designed to excite a mode orthogonal to the fundamental dipole mode that is excited by the monopole in the short edge. Thus, orthogonal radiation patterns are obtained and mutual coupling between the antennas is low. The SAR performance of this prototype will be compared with PA where the two monopoles excite the same characteristic mode.

6.4.1 Stand-Alone SAR

The SA-SAR values for the two prototypes at the low frequency band are shown in Fig. 39. In PA, the results are the same for the two ports since the antennas are identical. In PD, the actual distance between the antenna element and the flat phantom plays an important role on SAR values. For S1, the T-Strip antenna is further away from the phantom and the monopole is much closer so that the monopole (Port 1) produces a higher SAR value. The opposite behavior is expected for S2. Additionally, for PD, each port excitation does not affect the other due to low mutual coupling between the antennas.

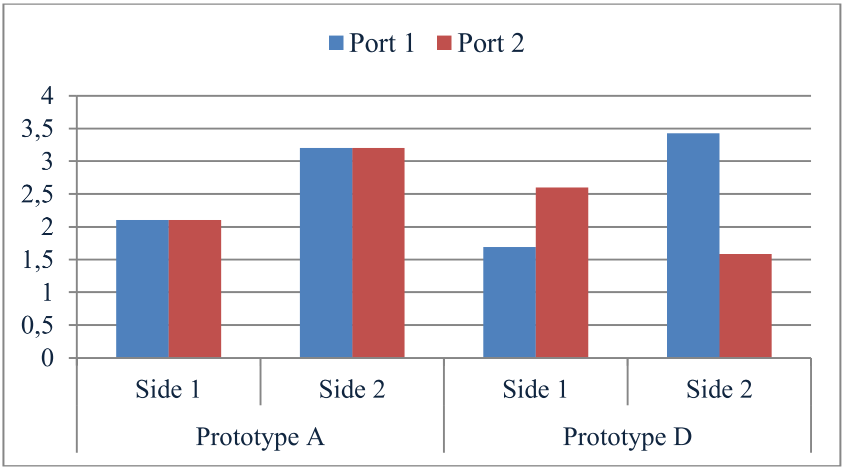

Figure 39: SA-SAR Prototypes A and D (0.859 GHz)

6.4.2 MIMO-SAR

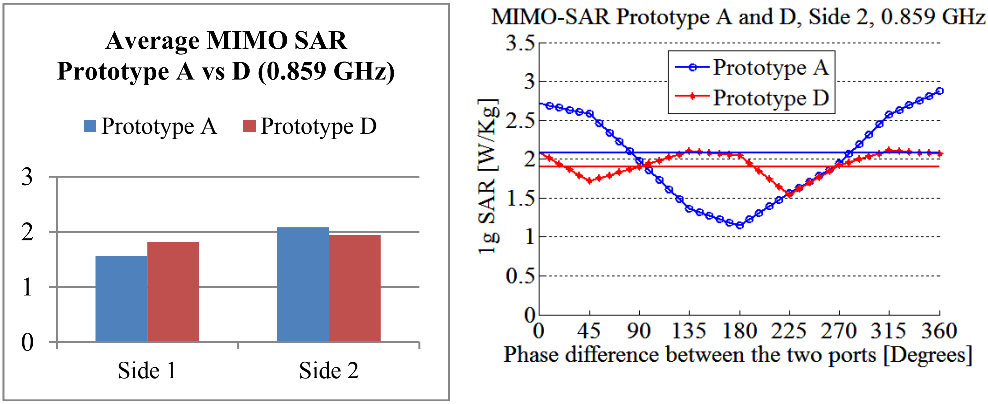

(a) (b)

Figure 40: MIMO-SAR behavior for PA and PD

When the prototypes are tested for MIMO-SAR, it is observed that despite these two schemes excite the chassis differently, their averaged MIMO-SAR values are similar at the low frequency band, as presented in Fig. 40(a). The other phenomenon is that PA gives a larger MIMO-SAR deviation from its average, while PD has a more stable overall behavior. This is also a result of the low mutual coupling between the two ports in PD where less power leaks from one port to the other. This makes the

MIMO-SAR almost constant over different phase shifts. As a newly proposed antenna setup, it is concluded that SAR values for PD are comparable, if not better than the traditional antenna setup. The other performances of PD, such as the correlation and efficiencies, are better than the traditional antennas, making it attactive as future mobile handset antennas.

Another interesting observation is the location of the hotspots for PD (see Fig. 41). The T-strip antenna behaves as a dipole along the width of the chassis in the case of PD-S2 in the low band. Unlike the other setups, the location of the hotspots in PD changes from one longer edge to the other when the phase shift varies from 0^o to 180^o. In the high band the hotspots moves across the short edges of the chassis.

MIMO-SAR trends for all prototypes are presented in Appendix A2.

PD-S2				
859 MHz			1.92 GHz	
$\Delta\varphi=0^o$	$\Delta\varphi=60^o$	$\Delta\varphi=160^o$	$\Delta\varphi=0^o$	$\Delta\varphi=180^o$

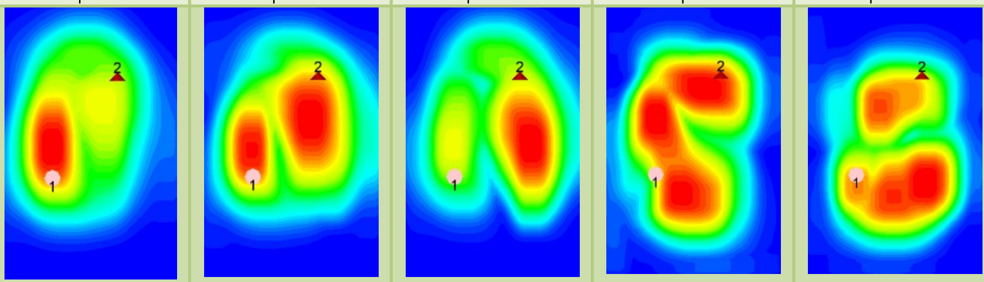

Figure 41: MIMO-SAR for Prototype D – Side 2

CHAPTER 7

7 Measurements with Flat Phantom

In this chapter, SAR measurement results for the fabricated handsets are presented; SA-SAR and MIMO-SAR were measured on the flat phantom for PA.

7.1 Power Monitoring

When it comes to actual measurements, one very important aspect is power monitoring. In real life, the antennas are not perfectly matched and there are losses between the feeding power and the power accepted by the antenna. Consequently we need to monitor and use the accepted power as the reference for consistency between the simulations and measurements. This power is normalized to 0.25 W and 0.13 W for the low and high bands, respectively.

Figure 42 shows the measurement setup: A signal generator creates the feeding signal that is amplified and passed through a directional coupler. A power monitor is used to monitor the required feeding power that will be used in the SAR calculation. For the MIMO-SAR measurements, a splitter is used to transmit equal power to the two ports.

The return loss in a transmission system is:

$$RL[dB] = 10log_{10}\frac{P_r}{P_i} = P_r[dB] - P_i[dB] \tag{4}$$

where P_r is the reflected power from the antenna and P_i is the incident (or stimulated) power that is fed to the antennas.

Moreover in linear scale:

$$RL = \frac{P_r}{P_i} \leftrightarrow P_r = P_i RL \tag{5}$$

The incident power P_i is defined as the sum of the accepted power P_{acc} and the reflected power P_r:

$$P_i = P_{acc} + P_r \leftrightarrow P_{acc} = P_i - P_r \tag{6}$$

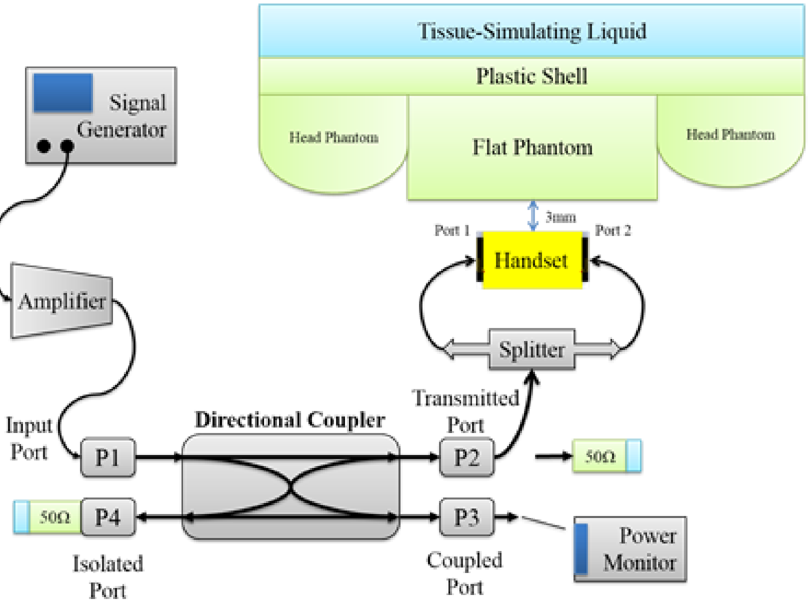

Figure 42: Measurement setup with the flat phantom

Thus, the accepted power is calculated as:

$$\overset{(5),(6)}{\Longrightarrow} P_{acc} = P_i - P_i RL = P_i(1 - RL) \tag{7}$$

The return loss RL can be found from (4) (see also Fig. 42):

$$P_i = P1 + (P2_{50\Omega} - P2_{ant}), \tag{8}$$

where $P1$ is the power applied at the input port directly after the amplifier, whereas $P2_{50\Omega}$ and $P2_{ant}$ are the monitored powers when $P2$ is loaded with 50 Ω and the antenna's match, respectively. Finally the reflected power P_r can be monitored from:

$$P_r = P3 + a_c \tag{9}$$

where P3 is the power monitored at Port 3 and a_c stands for the coupler's attenuation.

7.2 SAR Measurements in Flat Phantom

PA was the device under test in this measurement and a detailed view of the fabricated prototype can be seen in Fig. 43(a). The measurements were performed with a COMOSAR system from SATIMO, where a robotic arm is used to drive a probe into the liquid material [8] inside tank that has the shape of the flat phantom (see Fig. 43(b)-(d)). For the SA-SAR measurements one antenna is fed and the other is terminated with a 50 Ω load, whereas for the MIMO-SAR measurement the splitter divides the power equally into the two ports. In the MIMO-SAR measurement, the phase difference between the two ports is 0^{o}.

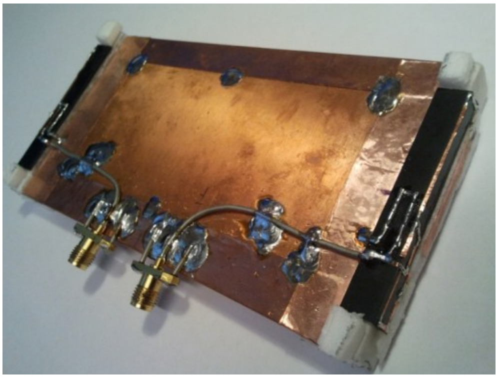

(a) Prototype A - fabricated handset

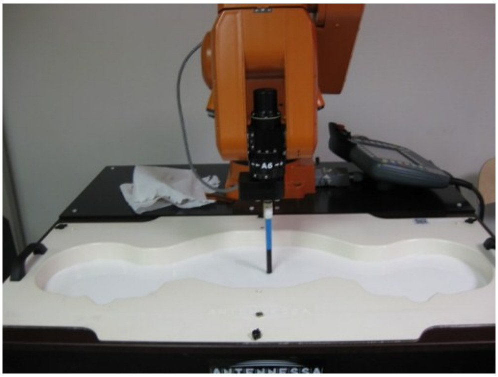

(b) The COMOSAR Robot System

(c) Prototype A -SAR measurement setup with Flat Phantom (SA-SAR)

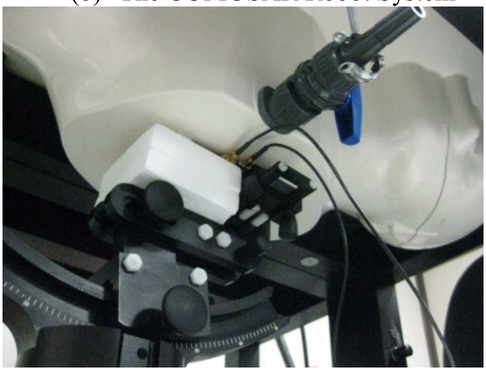

(d) Prototype A - SAR measurement setup with Flat Phantom (MIMO-SAR)

Figure 43: SAR measurements for Prototype A

The results from the measurements are compared with the simulations in terms of SAR distributions and SAR values.

Prototype A Measurements in COMOSAR – Side 1 (PA-S1)					
859 MHz			1.92 GHz		
Stand Alone SAR		MIMO SAR	Stand Alone SAR		MIMO SAR
Port 1	Port 2	$\Delta\varphi=0^{o}$	Port 1	Port 2	$\Delta\varphi=0^{o}$
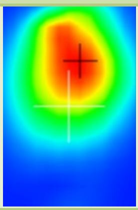	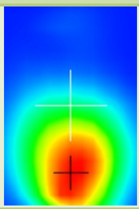	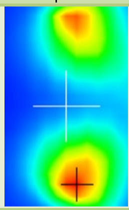	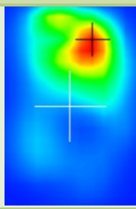	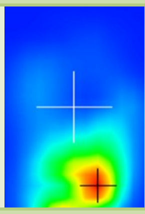	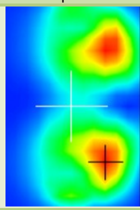
0.85 W/Kg	0.96 W/Kg	2.26 W/Kg	1.5 W/Kg	1.6 W/Kg	1.9 W/Kg

Figure 44

Prototype A Simulation in CST – Side 1 (PA-S1)					
859 MHz			1.92 GHz		
Stand Alone SAR		MIMO SAR	Stand Alone SAR		MIMO SAR
Port 1	Port 2	$\Delta\varphi=0^{o}$	Port 1	Port 2	$\Delta\varphi=0^{o}$
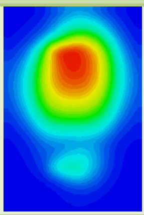	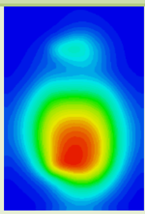	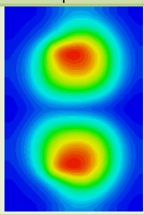	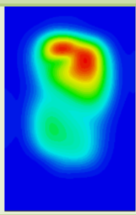	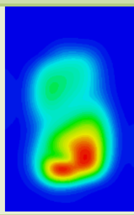	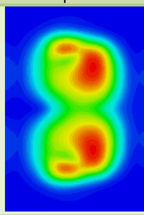
2.12 W/Kg	2.11 W/Kg	2.06 W/Kg	2.01 W/Kg	2,01 W/Kg	1.03 W/Kg

Figure 45

In Fig. 44, the measured SAR distributions for PA-S1 are presented, which agree well with the simulated distributions as shown in Fig. 45. The SAR values show some discrepancy since there are some differences between the ideal simulation and the practical measurement, including the input power, the liquid properties, the temperature and the dielectric losses in the prototypes.

Figure 46 shows the measurement and simulation results for PA-S2. As in the case of S1, good agreement can be seen between the simulated and measured results.

Prototype A Measurements in COMOSAR for SA-SAR – Side 2 (PA-S2)			
859 MHz		1.92 GHz	
Port 1	Port 2	Port 1	Port 2
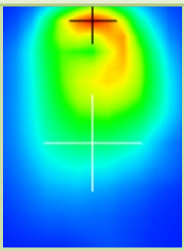	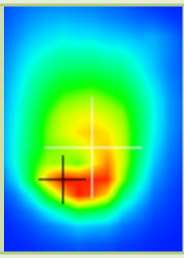	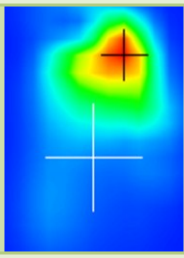	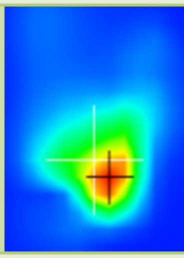
1.677 W/Kg	1.778 W/Kg	2.23 W/Kg	2.49 W/Kg
Prototype A Simulation in CST for SA-SAR – Side 2 (PA-S2)			
859 MHz		1.92 GHz	
Port 1	Port 2	Port 1	Port 2
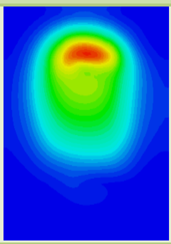	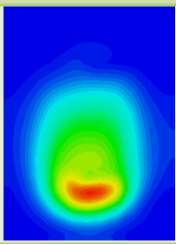	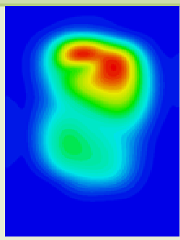	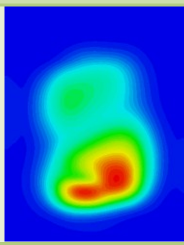
3.2 W/Kg	3.225 W/Kg	2.691 W/Kg	2.704 W/Kg

Figure 46

CHAPTER 8

8 Simulations with Head and Hand Phantom (Talking Mode)

Talking mode stands for the situation where a user holds the mobile phone while placing it near the head, for example while making a voice call. This talking mode is important for SAR evaluation, because of the proximity of the radiating elements to the human brain. Here, we will present the SAR simulation results in CST for PA, PB, PC and PD. The four prototypes are placed close to the head phantom that is also known as Specific Anthropomorphic Mannequin (SAM) as defined by IEEE SCC 34, on which all relevant radiation standards are based (e.g., CTIA). A hand phantom that surrounds the device is also included in the simulation since it impacts the antenna performance and therefore SAR.

8.1 Head and Hand Mannequins

In the CST software, the SAM head (see Fig. 47) is modeled by a shell that is filled with the liquid which represents the material of the head. The properties of the phantom head are shown in Table 5.

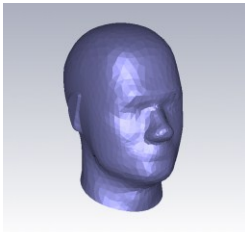

Figure 47: The Head Phantom

Table 5 : Simulated SAM Head Properties

	Relative Dielectric Constant ε_r	Conductivity σ [S/m]
Inner Liquid	42	0.99
Outer Shell	5	0.05
Quantity	5.3 Kg	

The existence of the hand and how the handset is held can influence SAR, so that it is important to include the hand in the simulation to emulate real life situations and provide meaningful assessments of the performance. A homogeneous mannequin of appropriate dielectric parameters is used in the simulation to represent the real hand. Its geometry is shown in Fig. 48, with the dielectric properties listed in Table 6.

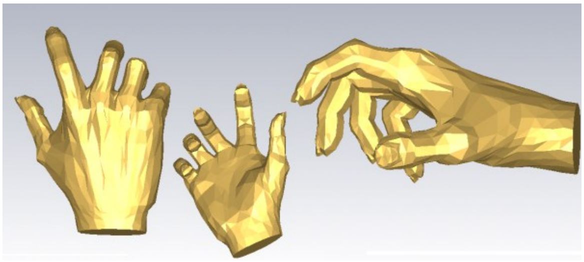

Figure 48: The Hand Phantom

Table 6 : Dielectric Properties of the SAM hand

Target Frequency [MHz]	ε´	ε´´
900	30	12.38
1450	27.9	10.54
1800	27	9.89
1900	26.7	9.84
2100	26.3	9.76
2450	25.7	9.68

8.2 Distance and Positioning

The distance between the prototype and the SAM head is defined as the vertical distance from the center of the top side of the mobile to the center of the right ear at the SAM head. Same as for the flat phantom, this distance is set to 3 mm. For the talking mode, it is always the screen side (S1) that is facing the head.

When the user is holding the mobile in the talking mode, the surface of the phantom is not flat anymore. The head has a geometrically uneven structure and exhibits anomalies as compared with the flat phantom. Moreover, the presence of the hand also affects the SAR, since it can reflect and absorb radiation from the prototype. The distance between the prototype and the head is not uniform, and it increases when it approaches the bottom of the prototype (see Fig. 49). Therefore, it is expected that the antennas at the bottom short edge of the chassis contribute less to the total SAR as compared with the ones near the top edge of the chassis.

The angle between the mobile phone and the human head is another important aspect. It has been reported in [5] that increasing the angle from 0 to 90 degrees leads to much higher SAR values. It means that better SAR values are obtained at 0 degrees where the mobile is in the vertical position. In this thesis work, the position of the mobile phone is aligned to the straight line between the ear and the mouth (see Fig. 49(c) for detail), which is the most common position in real life and stands between the extreme cases of [5].

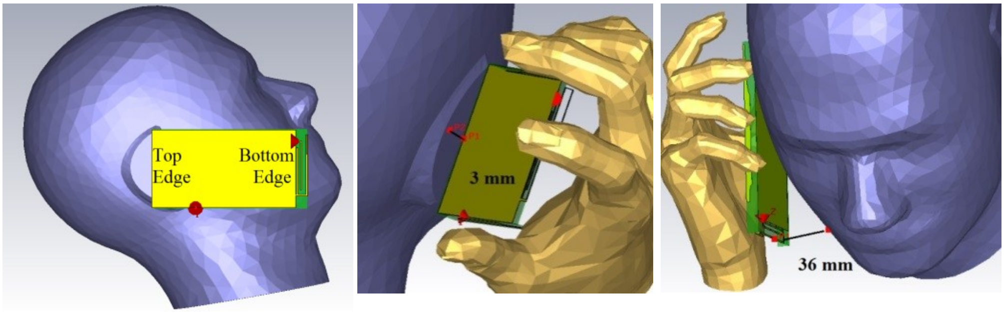

(a) Talking Mode Setup (b) Top Edge (c) Bottom Edge

Figure 49: Illustrative Example - Distance between Prototype D and the SAM head

8.3 Stand-Alone SAR

Prototype A – SA-SAR				
Set-up	859 MHz		1.92 GHz	
Side view	Port 1 Excitation	Port 2 Excitation	Port 1 Excitation	Port 2 Excitation
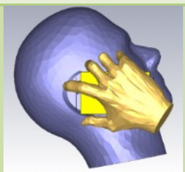	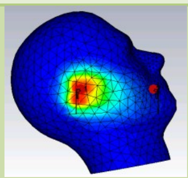	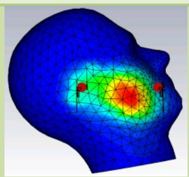	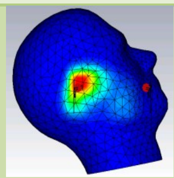	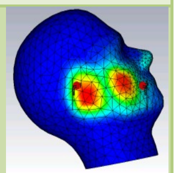
1 g SAR:	1.9925 W/Kg	0.6125 W/Kg	1.794 W/Kg	0.2964 W/Kg

Figure 50

We have seen from Chapter 6 that SA-SAR for PA exhibits a symmetric SAR distribution due to the identical antennas on the opposite short edges of the chassis. The results in Fig. 50 show that in the talking mode, the hotspot located close to the ear has much higher SAR value than the corresponding one at the bottom side due to the difference in the distance between the antennas and the head. The SAR distributions are no longer symmetrical for the same reason.

Prototype B – SA-SAR				
Set-up	859 MHz		1.92 GHz	
Side view	Port 1 Excitation	Port 2 Excitation	Port 1 Excitation	Port 2 Excitation
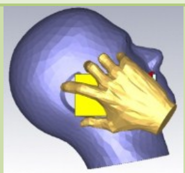	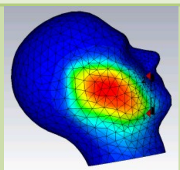	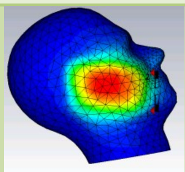	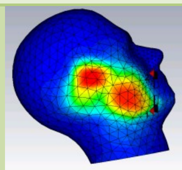	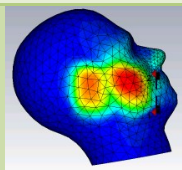
1 g SAR:	0.9375 W/Kg	1.01 W/Kg	0.5343 W/Kg	0.5252 W/Kg

Figure 51

Similar to PA, the SAR distribution for PB is not symmetric as well, as observed from Fig. 51. One important remark is that the SAR values for PB in the talking mode are reduced by more than 50% compared with the flat phantom case. In this set-up, both co-located antennas are placed at the bottom edges of the chassis and this corresponds to smaller SAR values, because of the larger distance between the antenna elements and the head.

Prototype C – SA-SAR				
Set-up	859 MHz		1.92 GHz	
Side view	Port 1 Excitation	Port 2 Excitation	Port 1 Excitation	Port 2 Excitation
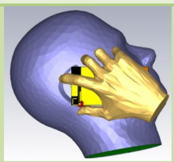	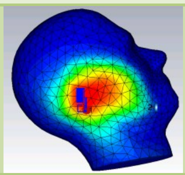	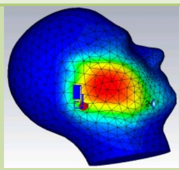	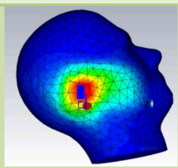	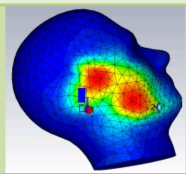
1 g SAR:	1.0075 W/Kg	1.0325 W/Kg	0.9126 W/Kg	0.4303 W/Kg

Figure 52

For PC-S1 in the talking mode, the PIFA (port 1) is placed at the top edge and it radiates away from the head due to the existence of the ground plane below the radiating element. The monopole (port 2) is located at the bottom of the mobile structure and again the SAR value is smaller because it is far from the chin.

Prototype D – SA-SAR				
Set-up	859 MHz		1.92 GHz	
Side view	Port 1 Excitation	Port 2 Excitation	Port 1 Excitation	Port 2 Excitation
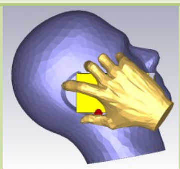	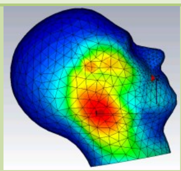	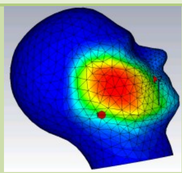	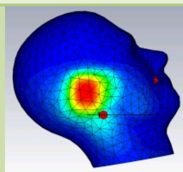	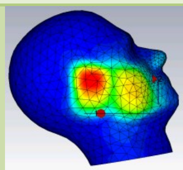
1 g SAR:	0.2925 W/Kg	0.7925 W/Kg	1.0985 W/Kg	0.6838 W/Kg

Figure 53

The SAR distribution for PD is different from the other prototypes. When port 1 (the T-strip antenna) is excited at 859 MHz, a very large SAR spread is observed and the SAR value is quite low (0.29 W/kg). The monopole, which is placed in the bottom of the chassis, also gives a low SAR value because of the large distance between the antenna and the chin. It is concluded that PD is much preferred for the talking mode from the perspective of SAR.

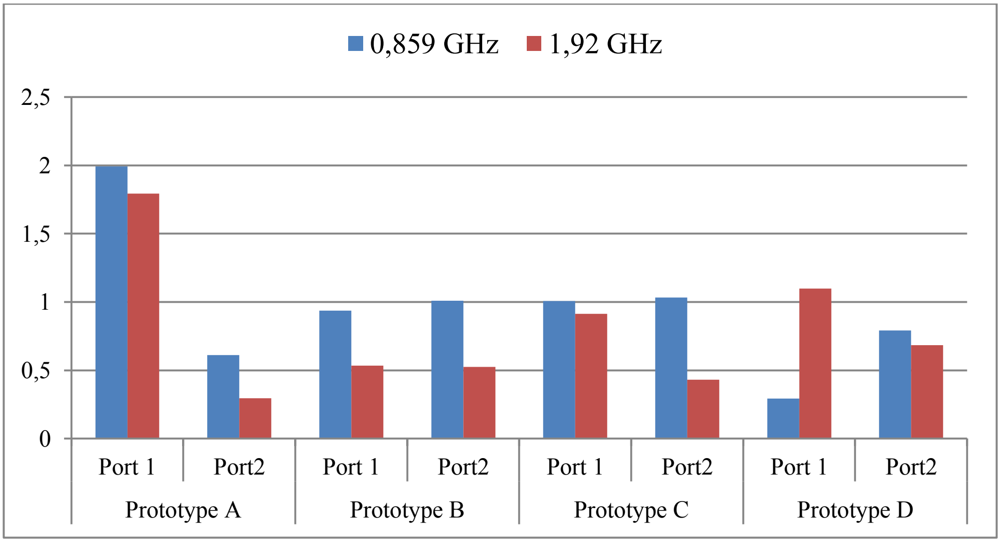

Figure 54: Stand Alone SAR - Talking Mode

Figure 54 gives an overview of the SA-SAR values for PA, PB, PC and PD in talking mode and summarizes our previous observations:

- Port 1 for PA generates the largest SAR because of the proximity of the monopole antenna to the ear.
- PB exhibits small SAR since both monopoles are located at the bottom side.
- For PC, the PIFA at the top side does not lead to a higher SAR value due to the existence of the ground plane between the PIFA and the head, while SAR from the monopole (port 2) is at low levels because it is further away from the chin.
- For PD, the T-strip antenna (port1) exhibits good behavior in the low band but gives a relatively higher SAR value at 1.92 GHz.

To ease comparison of results, Figs. 50-53 are also given in Appendix A3, but without the setup view.

8.4 MIMO-SAR

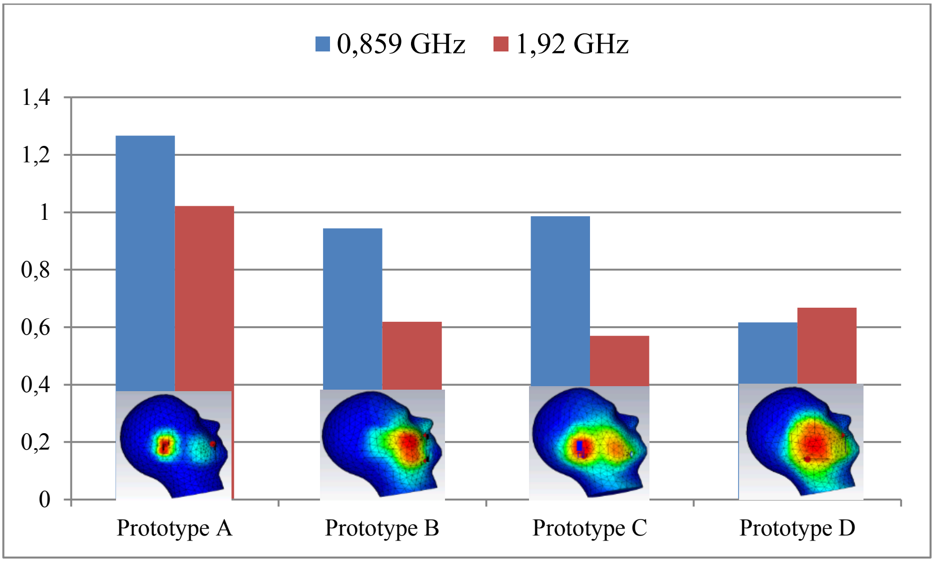

Figure 55: Average MIMO SAR - Talking Mode

The results for the averaged MIMO-SAR are shown in Fig. 55. Similar as the case of SA-SAR, PA gives the highest SAR values due to the effect of the top monopole. The remaining three prototypes produce good overall SAR (less than 1 W/kg), especially for PD. More details of the MIMO-SAR results are provided in Appendix A4.

CHAPTER 9

9 Conclusions

9.1 SAR with the Flat Phantom

The flat phantom is used for testing the radiation absorption when the user places the mobile device close to the body, which is referred to as the "Body-worn mode". This mode is preferred in the study of SAR distribution since the flat phantom is uniform and the influence of each antenna factor on SAR is more intuitive.

In general, when the SAR distribution is spread over a larger area, the peak SAR value is lower compared to the case where the hotspot is focused below the antenna element. The instantaneous MIMO-SAR value changes with respect to the phase difference between the signals in the two antenna ports.

When it comes to frequency of operation, in the high band, the SAR value will always be higher since the human body is more conductive at these frequencies and the current is more localized on the antenna. However, since the antennas are fed with less power (0.13 W) than at the low band (0.25 W), the final SAR values at most of the cases are lower than those at the 859 MHz band.

The effects of different antenna factors are summarized as follows:

- When antennas are placed at the short edge(s), the antenna location does not significantly affect SAR. The co-located and separated antenna setups exhibit similar SAR values and distributions because they excite the same characteristic mode of the chassis. The overall E-Field is almost identical in both cases, resulting in similar SA-SAR values and distributions. For MIMO-SAR the SAR distribution is not the same for the two setups when the phase difference between the two ports changes. However, the averaged MIMO-SAR values for both cases are similar.
- The antenna type plays an important role, especially when it comes to the prototype's orientation (two sides). Monopoles generate a more even SAR distribution regardless of the side due to their omnidirectional radiation. In the low band the current is flowing along the chassis and the whole device radiates as a dipole, whereas in the high band the current is more localized around the antennas.

For the on-ground PIFA, SAR values and distributions are different with respect to the different sides. The ground plane below the antenna plays an important role in the PIFA case.

- For different chassis mode excitations, i.e., the same chassis mode or two orthogonal chassis modes excited, the averaged MIMO-SAR values are similar, whereas the SA-SAR values depend on the design of each antenna, since the two antennas are not strongly coupled with each other. Taking advantage of the orthogonal modes of the chassis is a relatively new concept for multi-antenna design in mobile handsets, which can provide low mutual coupling and correlation between the antennas. While these are useful properties when it comes to MIMO performance in a mobile terminal, the SAR behavior of this newly proposed antenna is comparable to, if not better than, the conventional antenna setups. Actually, the SAR results in the talking mode show that PD leads to a lower SAR than the other antenna prototypes.

9.2 SAR with the Head and Hand Phantom

The head and hand phantoms are used in CST to simulate the case where a user performs a voice call with the phone, which is referred to as the "Talking Mode".

In this case, the distance between the head and the mobile device is not uniform, and it affects the SAR values. When the antenna is located at the bottom edge, the SAR value is lower due to the larger distance between the radiating element and the human body. The opposite happens when the antenna is at the top edge. Summarizing:

- PA, with identical monopoles located in the opposite edges of the chassis, gives the largest SAR values both for SA-SAR and MIMO-SAR. This is due to the proximity of one antenna element close to the head, which determines the overall performance and increases SAR.
- PB, composed of the co-located monopoles at the same bottom edge of the chassis, exhibits much lower SAR values compared with PA in the talking mode. Co-located setup saves precious space when it comes to mobile terminal design. It is also a good solution from the perspective of SAR since it reduces the radiation absorption in the talking mode and does not influence SAR values significantly in the body-worn mode.

- PC, with the on-ground PIFA at the top edge and the monopole at the bottom, was studied. The ground plane below the PIFA blocks the power absorbed by the head to some extent, decreasing SAR even though it is close to the head. Since PIFA is narrowband, it can be used as a diversity antenna, and the monopole as the main antenna at the bottom to ensure small SAR.
- Finally, PD exhibits quite low SAR in the talking mode, particularly for MIMO-SAR because the absorption is spread over a larger area.

9.3 Future Work

The electromagnetic absorption of a human body has always been not only an interesting but also an important topic. The recent deployment of multiple antennas in mobile terminals indicates that SAR should be studied in extended details when it comes to MIMO transmission. Since MIMO-SAR varies with different antenna design parameters, in-depth study can lead to reduction of the absorption according to optimization in antenna positioning, type and feeding. Moreover, new evaluation techniques should be developed and applied in the future.

For the MIMO-SAR measurement using the traditional system, the procedure requires quite some time for calibrating the equipment and monitoring the feeding power, Furthermore, a lot of care is needed to precisely position the prototypes close to the phantom. To reduce the measurement time and improve the accuracy of the measurement, measurements with the more advanced measurement system developed by ART-FI (i.e., ART-MAN) is planned for the future. This system consists of a novel RF probe-array measurement technology with high accuracy and fast result acquisition. Therefore, better agreement between the measured and simulated results can be expected.

References

[1] J. C. Lin, **"Specific Absorption Rates Induced in Head Tissues by Microwave Radiation from Cell Phones"**, IEEE Antennas and Propagation Magazine, vol. 42, no. 5, pp. 138-139, March 2001.

[2] C. H. Li, M. Douglas, E. Ofli, B. Derat, S. Gabriel, N. Chavannes, N. Kuster, **"Influence of the Hand on the Specific Absorption Rate in the Head"**, IEEE Transactions on Antennas and Propagation, vol. 60, no. 2, pp. 1066-1074, February 2012.

[3] K. Fujimoto, **"Mobile Antenna Systems Handbook"**, Artech House, 2008.

[4] P. Pinho, A. Lopes, J. Leite, J. Casaleiro, **"SAR Determination and Influence of the Human Head in the Radiation of a Mobile Antenna for two Different Frequencies"**, in Proceedings of the International Conference on Electromagnetics in Advanced Applications (ICEAA'09), pp. 431-434, September 2009.

[5] R. Hosseinzadeh, B. Zakeri, "**SAR of the Human's Head due to Electromagnetic Radiation of a Mobile Antenna"**, in Proceedings of the 20th IEEE Telecommunications Forum (TELFOR), pp. 1159-1161, November 2012.

[6] R. T. Becker, **"Precoding and Spatially Multiplexed MIMO in 3GPP Long-Term Evolution"**, High Frequency Electronics, pp. 18-26, October 2009.

[7] K. Zhao, S. Zhang, Z. Ying, T. Bolin, S. He, **"SAR Study of Different MIMO Antenna Designs for LTE Application in Smart Mobile Phones"**, in Proceedings of the IEEE Antennas and Propagation Society International Symposium (APSURSI), July 2012.

[8] K. Queveler, O. Meyer, B. Derat, T. Coradin, C. Bonhomme, **"Rational Chemical Design of Broadband Tissue-Simulating Liquids"**, Proceedings of BioEM'2013, Thessaloniki, Greece, 11 June 2013,

[9] H. Li, Y. Tan, B. K. Lau, Z. Ying, S. He, **"Characteristic Mode based Tradeoff Analysis of Antenna Chassis Interactions for Multiple**

Antenna Terminals", IEEE Transactions on Antennas and Propagation, vol. 60, no 2, pp. 490-502, February 2012

[10] FCC Encyclopedia, Broadband Personal Communications Service, http://www.fcc.gov/encyclopedia/broadband-personal-communications-service-pcs

[11] H. Li, B. K. Lau, Z. Ying, S. He **"Decoupling of Multiple Antennas in Terminals With Chassis Excitation using Polarization Diversity, Angle Diversity and Current Control",** IEEE Transactions on Antennas and Propagation, vol. 60, no 12, pp. 5947-5957, December 2012.

[12] V. Plicanic, B. K. Lau, A. Derneryd, Z. Ying, **"Actual Diversity Performance of a Multiband Diversity Antenna with Hand and Head Effects",** IEEE Transactions on Antennas and Propagation, vol. 57, no. 2, pp. 1547-1556, May 2009.

[13] Z. Miers, H. Li, B. K. Lau **"Design of Bandwidth Enhanced and Multiband MIMO Antennas Using Characteristic Modes",** IEEE Antennas Wireless Propagation Letters, vol. 12, pp. 1696-1699, 2013.

[14] K. Zhao, S. Zhang, Z. Ying, T. Bolin, S. He, **"SAR Study of Different MIMO Antenna Designs for LTE Application in Smart Mobile Handsets"**, IEEE Transactions on Antennas and Propagation, vol. 61, no. 6, pp. 3270-3279, June 2013.

[15] M. Zhang, T. Wittig, A. Prokop, "**Application of CST Time Domain Algorithm in the Electromagnetic Simulation Standard of the SAR for Mobile Phone"**, in Proceedings of the International Conference on Microwave and Millimeter Wave Technology (ICMMT'2008), vol. 4, pp. 1717-1720, April 2008.

[16] Federal Communications Commission Office of Engineering & Technology, **"Evaluating Compliance with FCC Guidelines for Human Exposure to Radiofrequency Electromagnetic Fields"**, Supplement C (Edition 01-01) to OET Bulletin (65 Edition 97-01), June 2001.

[17] M. S. Wang, L. Lin, J. Chen, D. Jackson, W. Kainz, Y. H. Qi, P. Jarmuszewski, **"Evaluation and Optimization of the Specific Absorption**

Rate for Multiantenna Systems", IEEE Transactions on Electromagnetic Compatibility, vol. 53, no. 3, pp. 628-637, August 2011.

[18] R. F. Harrington, J. R. Mautz, **"Theory of Characteristic Modes for Conducting Bodies"**, IEEE Transactions on Antennas and Propagation, vol. 19, no. 5, pp. 622-638, September 1971.

[19] V. Plicanic, B. K. Lau, Z. Ying, "**Performance of Multiband Diversity Antenna with Hand Effects"**, in Proceedings of the International Workshop on Antenna Technology (iWAT'2008), pp. 534-537, March 2008.

[20] C.-H. Li, E. Ofli, N. Chavannes, N. Kuster, **"Effects of Hand Phantom on Mobile Phone Antenna Performance"**, IEEE Transactions on Antennas and Propagation, vol. 57, no. 9, pp. 2763-2770, September 2009.

[21] G. A. Kaatze, R. Behrends, R. Pottel, **"Hydrogen Network Fluctuations and Dielectric Spectrometry of Liquids",** Journal of Non-Crystalline Solids, vol. 305, pp. 19-28, 2002.

Related Material

[22] T. Wittig, **“SAR Overview”,** in Proceedings of the 3rd European User Group Meeting Technical Sessions, 2007. Available Online: http://www.cst.com/Content/Documents/Events/UGM2007/05-Wittig.pdf

[23] N. Perentos, S. Iskra, A. Faraone, R. J. McKenzie, G. Bit-Babik, V. Anderson, “**Exposure Compliance Methodologies for Multiple Input Multiple Output (MIMO) Enabled Networks and Terminals”**, IEEE Transactions on Antennas and Propagation, vol. 60, pp. 644-653, February 2012.

[24] C. T. Famdie, W. L Schroeder, K. Solbach, “**Numerical Analysis of Characteristic Modes on the Chassis of Mobile Phones”**, in Proceedings of the First European Conference on Antennas and Propagation, November 2006.

[25] N.V. Gritsenko, R.S. Zaridze, “**Influence of the Distance from the Mobile Antenna to Head on the SAR Investigation”**, in Proceedings of DIPED’2003, pp. 155-158, September 2003.

Appendix

The simulated SAR values that are presented below are normalized to comply with the limits of the regulations regarding the feeding power. The accepted power to the antennas is 0.25 W for 0.859 MHz and 0.13 W for 1.92 MHz. For clarity and comparison of the different absorption levels at each frequency band, SAR results for 1 W accepted power are presented as well.

A.1 Stand-Alone SAR in Flat Phantom

Prototype A

Side 1 (PA-S1)					
Set-up (3 mm)		859 MHz		1.92 GHz	
Side view	Top view	Port 1 Excitation	Port 2 Excitation	Port 1 Excitation	Port 2 Excitation
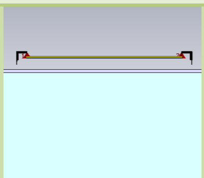	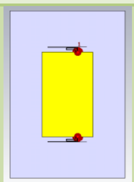	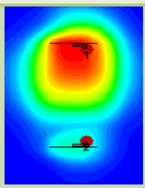	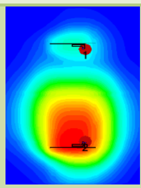	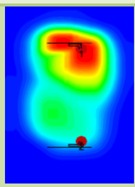	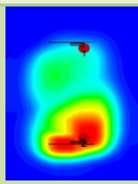
SAR (1 W)		8.5 W/Kg	8.45 W/Kg	15.5 W/Kg	15.5 W/Kg
SAR (0.25 W / 0.13 W)		2.125 W/Kg	2.1125 W/Kg	2.015 W/Kg	2.015 W/Kg

Side 2 (PA-S2)					
Set-up (3 mm)		859 MHz		1.92 GHz	
Side view	Top view	Port 1 Excitation	Port 2 Excitation	Port 1 Excitation	Port 2 Excitation
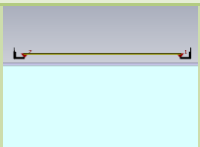	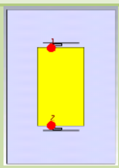	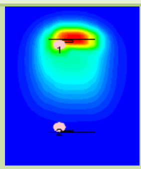	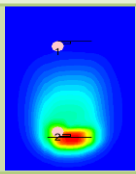	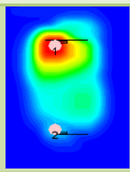	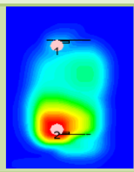
SAR (1 W)		12.8 W/Kg	12.9 W/Kg	20.7 W/Kg	20.8 W/Kg
SAR (0.25 W / 0.13 W)		3.2 W/Kg	3.225 W/Kg	2.691 W/Kg	2.704 W/Kg

Prototype B

Side 1 (PB-S1)					
Set-up (3 mm)		859 MHz		1.92 GHz	
Side view	Top view	Port 1 Excitation	Port 2 Excitation	Port 1 Excitation	Port 2 Excitation
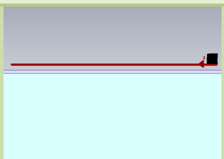	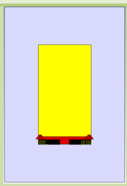	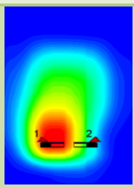	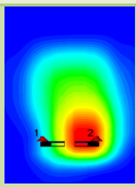	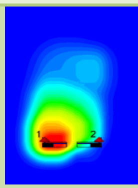	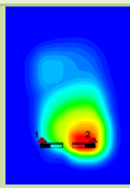
SAR (1 W)		10.3 W/Kg	10.3 W/Kg	28.2 W/Kg	28.2 W/Kg
SAR (0.25 W / 0.13 W)		2.57 W/Kg	2.57 W/Kg	3.7 W/Kg	3.7 W/Kg

Side 2 (PB-S2)					
Set-up (3 mm)		859 MHz		1.92 GHz	
Side view	Top view	Port 1 Excitation	Port 2 Excitation	Port 1 Excitation	Port 2 Excitation
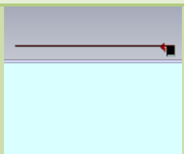	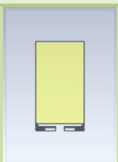	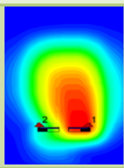	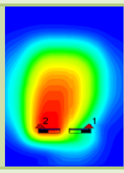	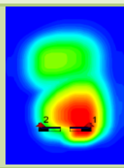	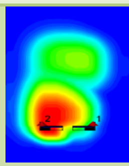
SAR (1 W)		5.9 W/Kg	5.91 W/Kg	10.5 W/Kg	10.5 W/Kg
SAR (0.25 W / 0.13 W)		1.47 W/Kg	1.47 W/Kg	1.36 W/Kg	1.365 W/Kg

Prototype B2

Side 1 (PB2-S1)					
Set-up (3 mm)		859 MHz		1.92 GHz	
Side view	Top view	Port 1 Excitation	Port 2 Excitation	Port 1 Excitation	Port 2 Excitation
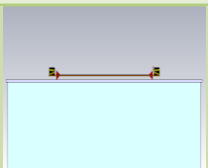	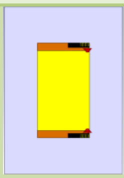	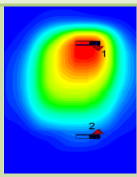	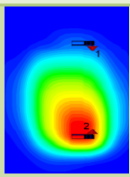	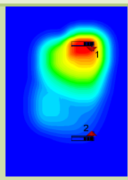	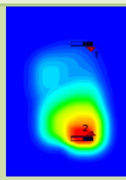
SAR (1 W)		9.32 W/Kg	9.32 W/Kg	28 W/Kg	28 W/Kg
SAR (0.25 W / 0.13 W)		2.33 W/Kg	2.33 W/Kg	3.64 W/Kg	3.64 W/Kg

Side 2 (PB2-S2)					
Set-up (3 mm)		859 MHz		1.92 GHz	
Side view	Top view	Port 1 Excitation	Port 2 Excitation	Port 1 Excitation	Port 2 Excitation
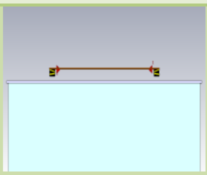	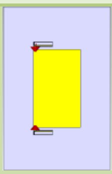	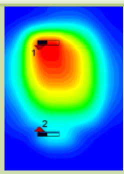	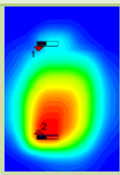	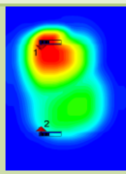	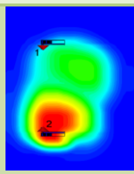
SAR (1 W)		6.94 W/Kg	6.94 W/Kg	12.1 W/Kg	12.1 W/Kg
SAR (0.25 W / 0.13 W)		1.73 W/Kg	1.73 W/Kg	1.57 W/Kg	1.57 W/Kg

Prototype C

Side 1 (PC-S1)					
Set-up (3 mm)		859 MHz		1.92 GHz	
Side view	Top view	Port 1 Excitation	Port 2 Excitation	Port 1 Excitation	Port 2 Excitation
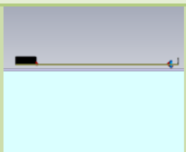	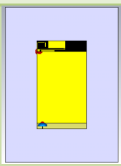	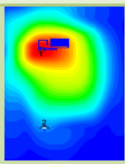	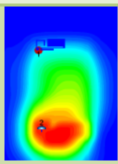	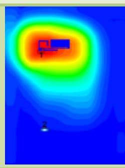	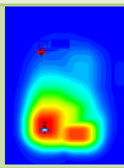
SAR (1 W)		6.58 W/Kg	9.17 W/Kg	12.3 W/Kg	19.1 W/Kg
SAR (0.25 W / 0.13 W)		1.67 W/Kg	2.29 W/Kg	1.59 W/Kg	2.48 W/Kg

Side 2 (PC-S2)					
Set-up (3 mm)		859 MHz		1.92 GHz	
Side view	Top view	Port 1 Excitation	Port 2 Excitation	Port 1 Excitation	Port 2 Excitation
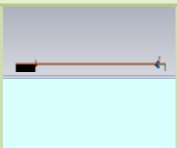	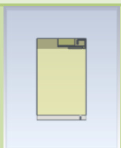	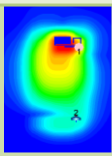	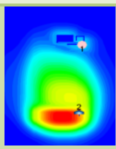	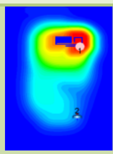	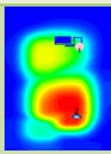
SAR (1 W)		11.9 W/Kg	13.4 W/Kg	18.7 W/Kg	9.87 W/Kg
SAR (0.25 W / 0.13 W)		2.79 W/Kg	3.35 W/Kg	2.41 W/Kg	1.28 W/Kg

Prototype D

Side 1 (PD-S1)					
Set-up (3 mm)		859 MHz		1.92 GHz	
Side view	Top view	Port 1 Excitation	Port 2 Excitation	Port 1 Excitation	Port 2 Excitation
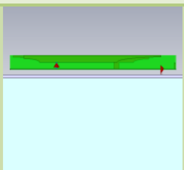	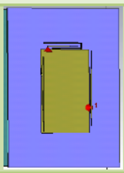	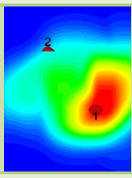	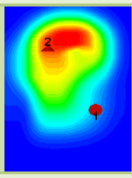	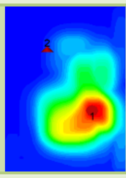	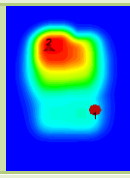
SAR (1 W)		6.75 W/Kg	10.4 W/Kg	12.9 W/Kg	19.2 W/Kg
SAR (0.25 W / 0.13 W)		1.68 W/Kg	2.6 W/Kg	1.67 W/Kg	2.49 W/Kg

Side 2 (PD-S2)					
Set-up (3 mm)		859 MHz		1.92 GHz	
Side view	Top view	Port 1 Excitation	Port 2 Excitation	Port 1 Excitation	Port 2 Excitation
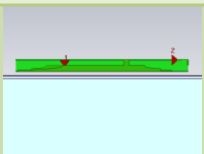	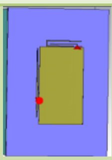	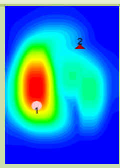	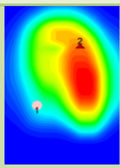	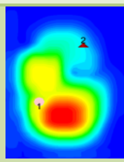	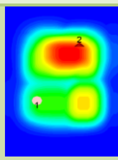
SAR (1 W)		13.7 W/Kg	6.53 W/Kg	9.09 W/Kg	9.52 W/Kg
SAR (0.25 W / 0.13 W)		3.42W/Kg	1.58 W/Kg	1.18 W/Kg	1.23 W/Kg

A.2 MIMO-SAR in Flat Phantom

Prototype A

Side 1 - 0.859 GHz (PA-S1-L)					
Side view	Top view	Δφ=0°	Δφ=90°	Δφ=180°	Δφ=270°
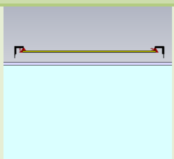	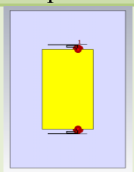	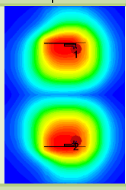	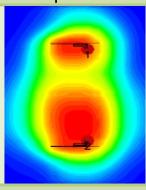	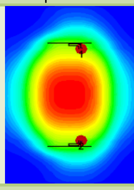	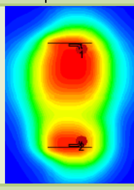
SAR (1 W)		8.25 W/Kg	5.2 W/Kg	5.44 W/Kg	5.11 W/Kg
SAR (0.25 W)		2.06 W/Kg	1.3 W/Kg	1.36 W/Kg	1.2775 W/Kg

Side 1 – 1.92 GHz (PA-S1-H)					
Side view	Top view	Δφ=0°	Δφ=90°	Δφ=180°	Δφ=270°
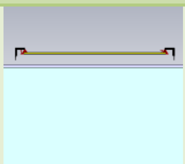	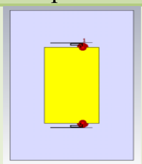	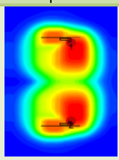	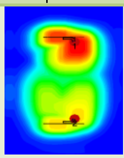	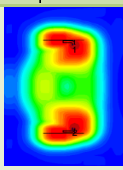	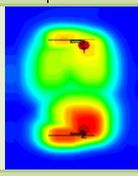
SAR (1 W)		7.94 W/Kg	10.9 W/Kg	9.24 W/Kg	10.8 W/Kg
SAR (0.13 W)		1.0322	1.417 W/Kg	1.2012 W/Kg	1.404 W/Kg

Side 2 - 0.859 GHz (PA-S2-L)					
Side view	Top view	Δφ=0°	Δφ=90°	Δφ=180°	Δφ=270°
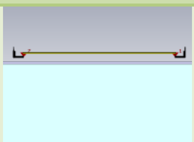	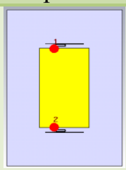	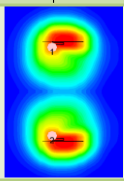	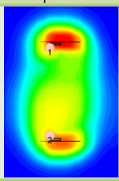	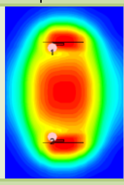	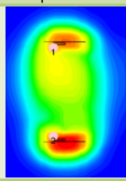
SAR (1 W)		10.8 W/Kg	7.78 W/Kg	4.55 W/Kg	7.71 W/Kg
SAR (0.25 W)		2.7 W/Kg	1.945 W/Kg	1.13 W/Kg	1.92 W/Kg

Side 2 - 1.92 GHz (PA-S2-H)					
Side view	Top view	Δφ=0°	Δφ=90°	Δφ=180°	Δφ=270°
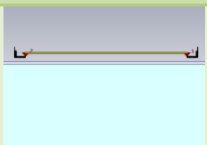	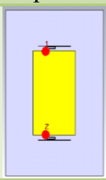	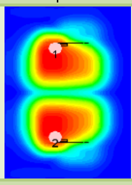	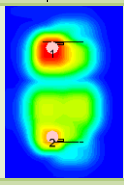	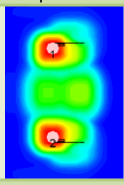	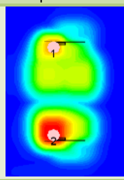
SAR (1 W)		8.59 W/Kg	13.8 W/Kg	15 W/Kg	13.8 W/Kg
SAR (0.13 W)		1.11 W/Kg	1.79 W/Kg	1.95 W/Kg	1.79 W/Kg

Prototype B

Side 1 - 0.859 GHz (PB-S1-L)					
Side view	Top view	Δφ=0°	Δφ=90°	Δφ=180°	Δφ=270°
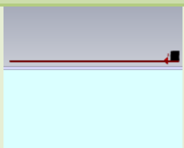	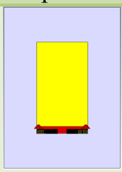	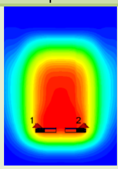	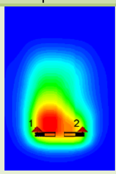	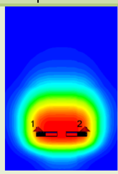	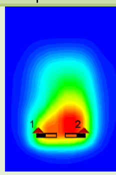
SAR (1 W)		4.83 W/Kg	6.78 W/Kg	10.8 W/Kg	6.99 W/Kg
SAR (0.25 W)		1.20 W/Kg	1.69 W/Kg	2.7 W/Kg	1.74 W/Kg

Side 1 – 1.92 GHz (PB-S1-H)					
Side view	Top view	Δφ=0°	Δφ=90°	Δφ=180°	Δφ=270°
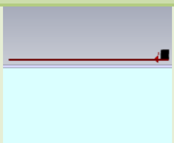	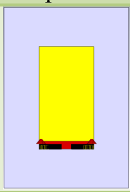	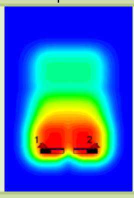	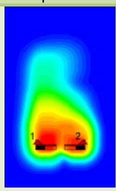	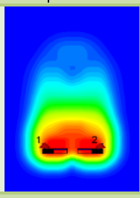	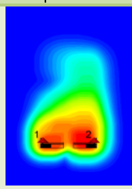
SAR (1 W)		13.5 W/Kg	16.6 W/Kg	16.7 W/Kg	16.6 W/Kg
SAR (0.13 W)		1.75 W/Kg	2.15 W/Kg	2.17 W/Kg	2.15 W/Kg

Side 2 - 0.859 GHz (PB-S2-L)					
Side view	Top view	Δφ=0°	Δφ=90°	Δφ=180°	Δφ=270°
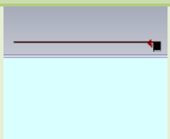	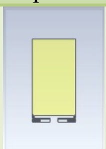	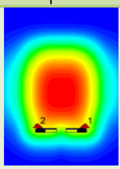	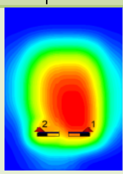	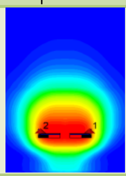	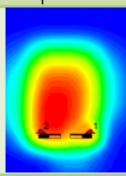
SAR (1 W)		4.59 W/Kg	4.78 W/Kg	8.22 W/Kg	4.97 W/Kg
SAR (0.25 W)		1.14 W/Kg	1.19 W/Kg	2.05 W/Kg	1.24 W/Kg

Side 2 – 1.92 GHz (PB-S2-H)					
Side view	Top view	Δφ=0°	Δφ=90°	Δφ=180°	Δφ=270°
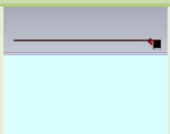	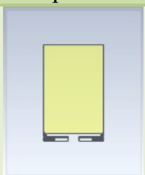	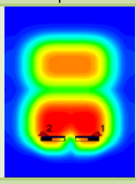	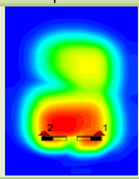	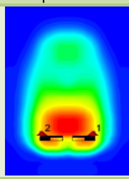	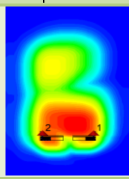
SAR (1 W)		6.91 W/Kg	8.38 W/Kg	9.85 W/Kg	8.32 W/Kg
SAR (0.13 W)		0.89 W/Kg	1.08 W/Kg	1.28 W/Kg	1.08 W/Kg

Prototype C

Side 2 - 0.859 GHz (PC-S2-L)					
Side view	Top view	Δφ=0°	Δφ=90°	Δφ=180°	Δφ=270°
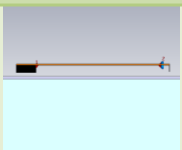	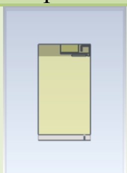	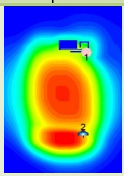	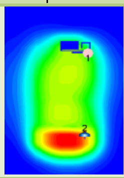	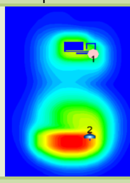	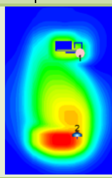
SAR (1 W)		5.71 W/Kg	10.1 W/Kg	16.9 W/Kg	10.3 W/Kg
SAR (0.25 W)		1.42 W/Kg	2.52 W/Kg	4.25 W/Kg	2.57 W/Kg

Side 2 - 1.92 GHz (PC-S2-H)					
Side view	Top view	Δφ=0°	Δφ=90°	Δφ=180°	Δφ=270°
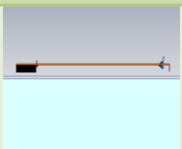	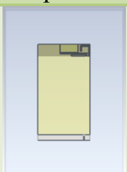	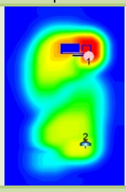	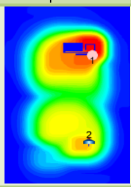	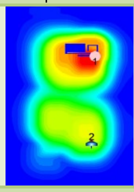	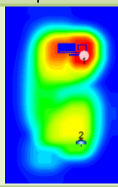
SAR (1 W)		13.3 W/Kg	9.63 W/Kg	12.1 W/Kg	11.7 W/Kg
SAR (0.13 W)		1.72 W/Kg	1.25 W/Kg	1.57 W/Kg	1.52 W/Kg

Prototype D

Side 2 - 0.859 GHz (PD-S2-L)					
Side view	Top view	Δφ=0°	Δφ=90°	Δφ=180°	Δφ=270°
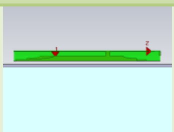	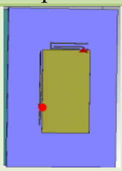	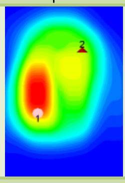	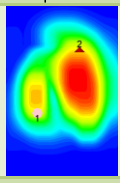	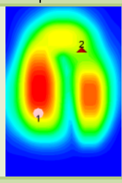	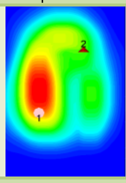
SAR (1 W)		8.43 W/Kg	7.78 W/Kg	7.42 W/Kg	8.29 W/Kg
SAR (0.25 W)		2.10W/Kg	1.94 W/Kg	1.85 W/Kg	2.07 W/Kg

Side 2 - 1.92 GHz (PD-S2-H)					
Side view	Top view	Δφ=0°	Δφ=90°	Δφ=180°	Δφ=270°
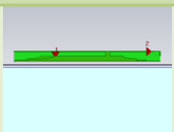	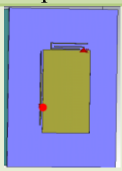	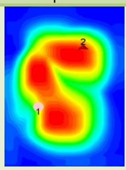	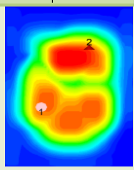	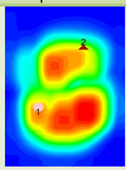	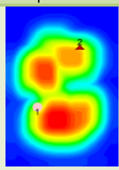
SAR (1 W)		5.95 W/Kg	5.7 W/Kg	6.84 W/Kg	6.86 W/Kg
SAR (0.13 W)		0.77 W/Kg	0.74 W/Kg	0.88 W/Kg	0.89 W/Kg

MIMO-SAR trends in Flat Phantom

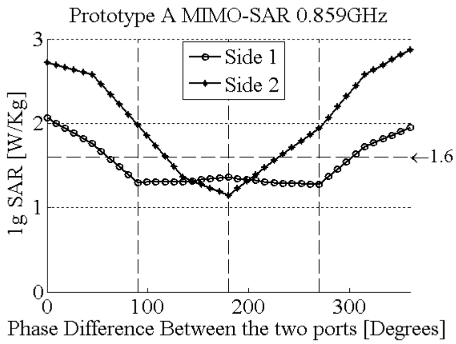

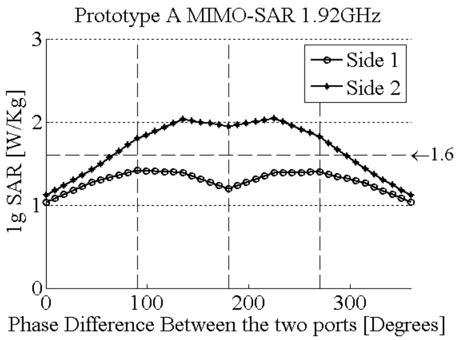

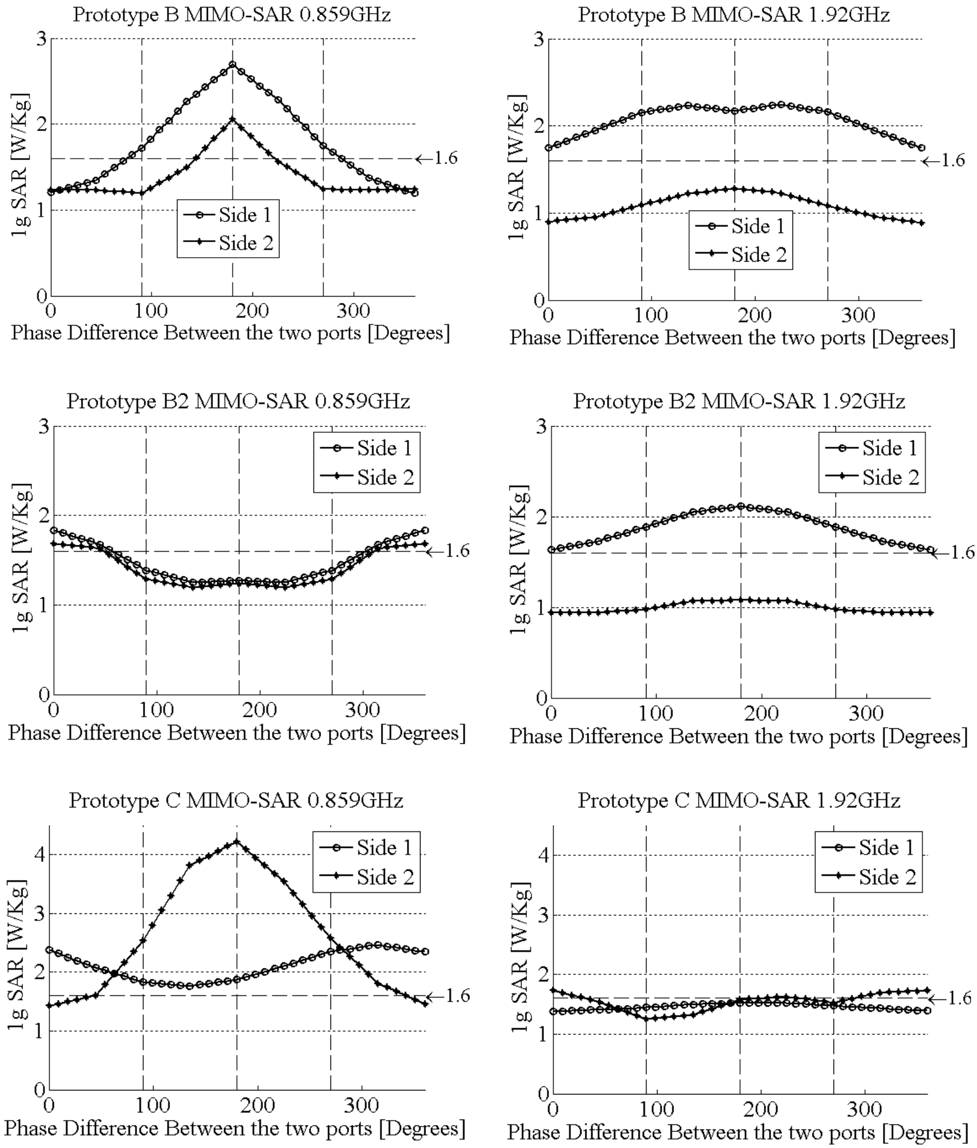
Prototype B MIMO-SAR 0.859GHz
Prototype B MIMO-SAR 1.92GHz
Prototype B2 MIMO-SAR 0.859GHz
Prototype B2 MIMO-SAR 1.92GHz
Prototype C MIMO-SAR 0.859GHz
Prototype C MIMO-SAR 1.92GHz
1g SAR [W/Kg]
Phase Difference Between the two ports [Degrees]
Side 1
Side 2
←1.6

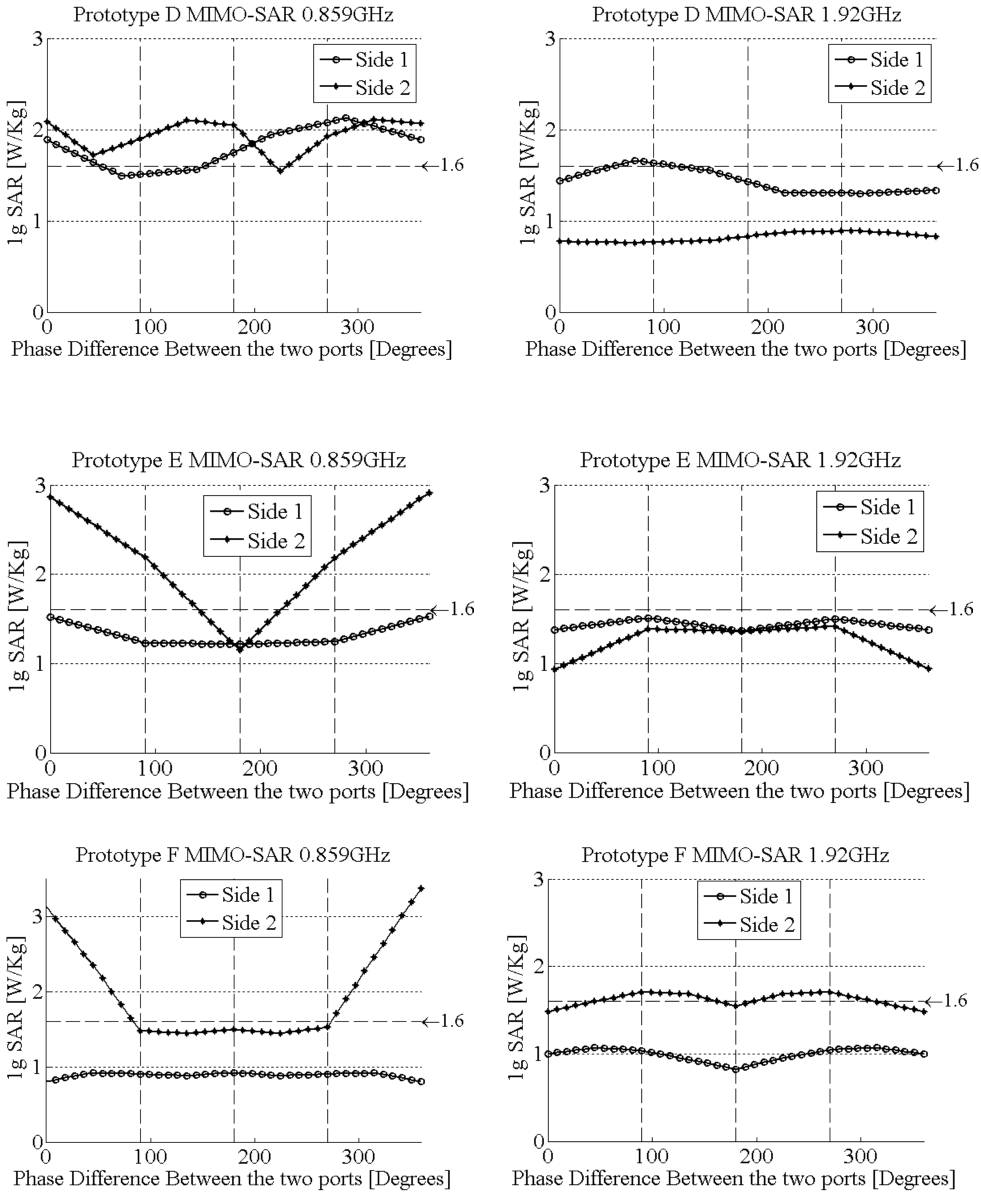
Prototype D MIMO-SAR 0.859GHz
Prototype D MIMO-SAR 1.92GHz
Prototype E MIMO-SAR 0.859GHz
Prototype E MIMO-SAR 1.92GHz
Prototype F MIMO-SAR 0.859GHz
Prototype F MIMO-SAR 1.92GHz
Side 1
Side 2
1g SAR [W/Kg]
Phase Difference Between the two ports [Degrees]
1.6
0
1
2
3
100
200
300

SPLSR example for D > 5 cm

For Prototype A (PA) we investigate the following set-up:

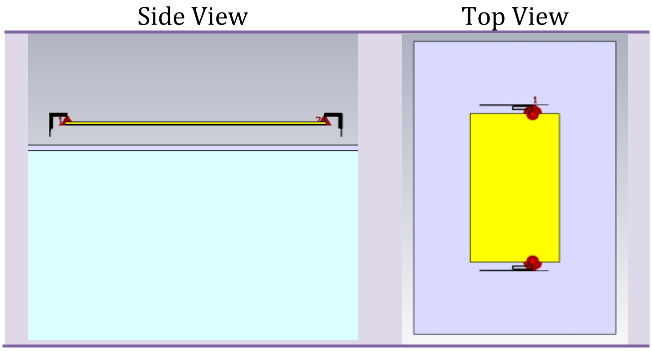

Side 1, 0.859 GHz (PA-S1-L)

The figure below shows the level of SAR value inside the flat phantom for the PA-S1-L set-up. The minimum ($\Delta\varphi=180^o$, black) and maximum ($\Delta\varphi=0^o$, red) MIMO-SAR values are included in this figure along with the SA-SAR of P1 and P2 (green and blue curves respectively); the yellow grid represents an upper bound for SAR when adding the fields generated from P1 and P2 together.

For PA-S1, the distance between the hotspots for SA-SAR is measured to be 11.56 cm and is larger than the 5 cm SPLSR limit. In this case we can observe that the maximum MIMO-SAR value (red curve) is not higher than the SA-SAR values (green, blue curves). There is no need for simultaneous transmission (both ports) measurement in this case.

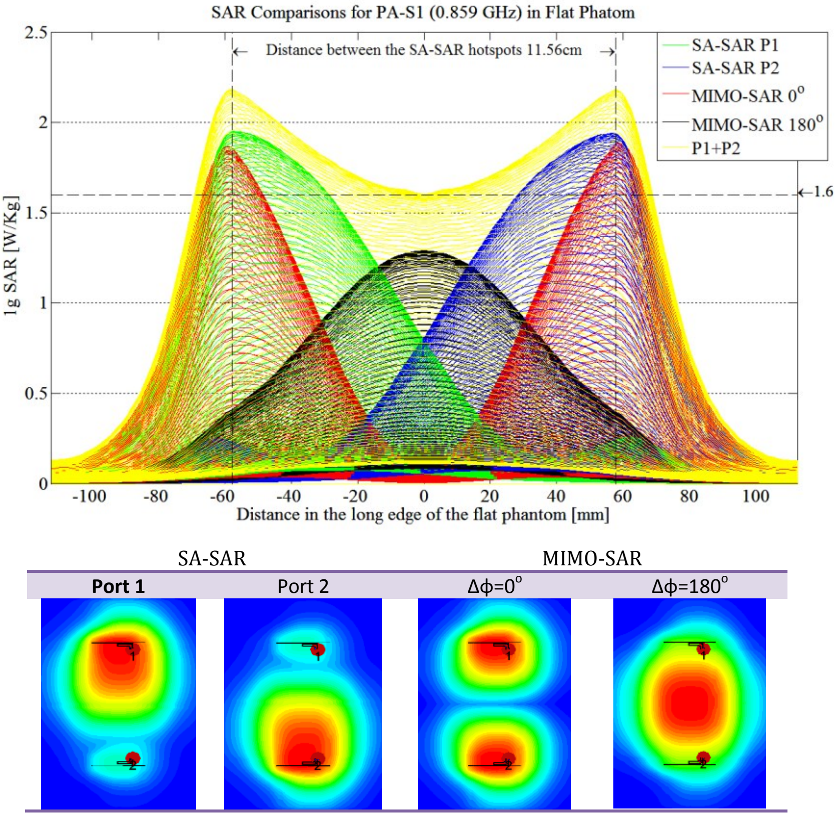

PA-S1-L SAR field distributions inside the flat phantom

Comparison between Average and Maximum MIMO-SAR

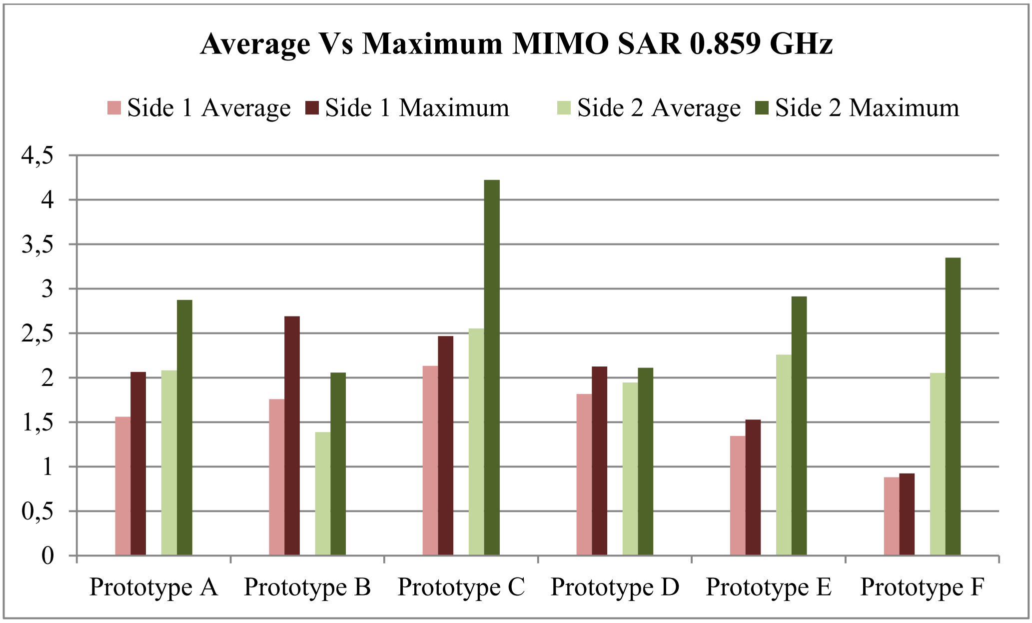

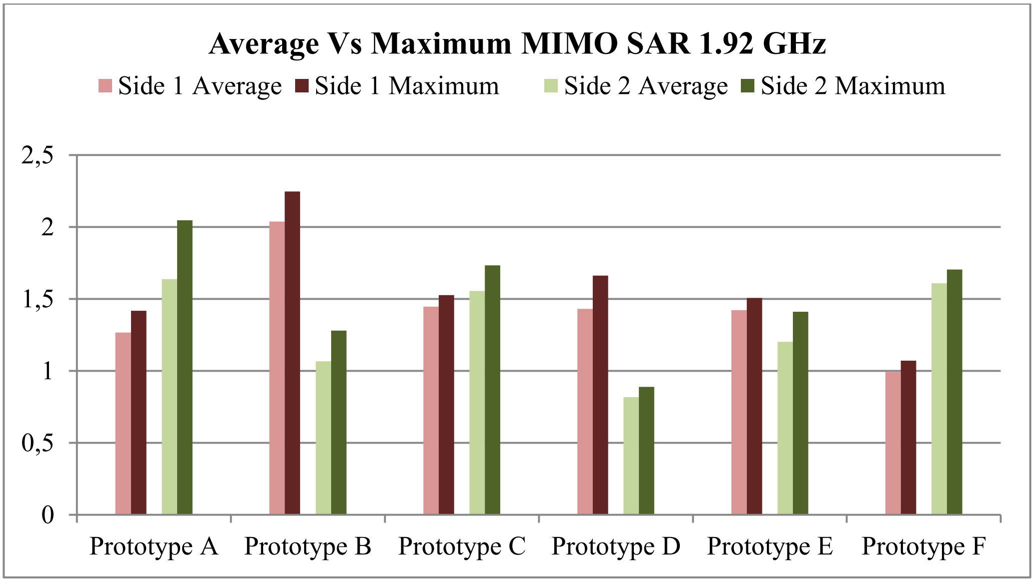

A.3 Stand-Alone SAR with Head and Hand Phantom

Prototype A			
859 MHz – 0.25 W accepted power		1.92 GHz - 0.13 W accepted power	
Port 1 Excitation	Port 2 Excitation	Port 1 Excitation	Port 2 Excitation
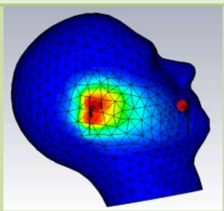	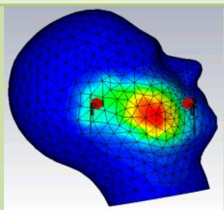	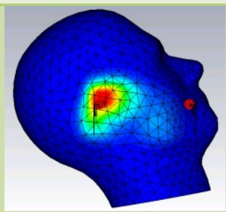	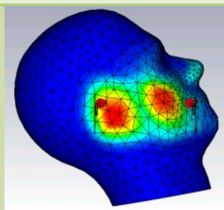
1.9925 W/Kg	0.6125 W/Kg	1.794 W/Kg	0.2964 W/Kg

Prototype B			
859 MHz – 0.25 W accepted power		1.92 GHz - 0.13 W accepted power	
Port 1 Excitation	Port 2 Excitation	Port 1 Excitation	Port 2 Excitation
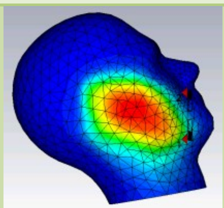	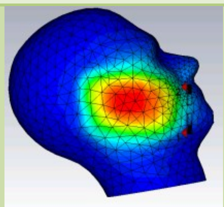	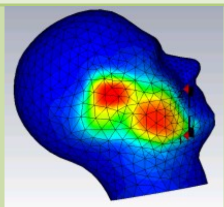	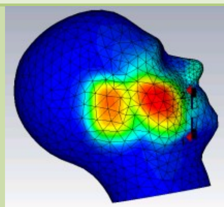
0.9375 W/Kg	1.01 W/Kg	0.5343 W/Kg	0.5252 W/Kg

Prototype C			
859 MHz – 0.25 W accepted power		1.92 GHz - 0.13 W accepted power	
Port 1 Excitation	Port 2 Excitation	Port 1 Excitation	Port 2 Excitation
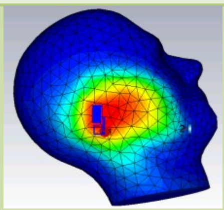	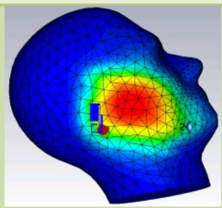	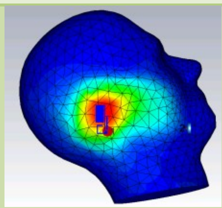	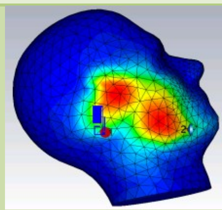
1.0075 W/Kg	1.0325 W/Kg	0.9126 W/Kg	0.4303 W/Kg

Prototype D			
859 MHz – 0.25 W accepted power		1.92 GHz - 0.13 W accepted power	
Port 1 Excitation	Port 2 Excitation	Port 1 Excitation	Port 2 Excitation
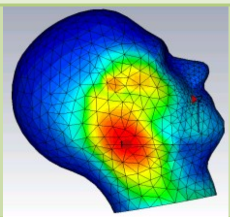	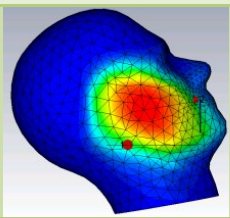	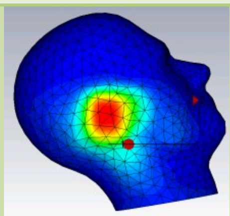	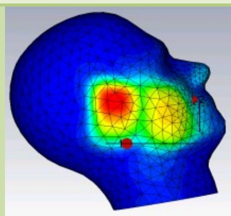
0.2925 W/Kg	0.7925 W/Kg	1.0985 W/Kg	0.6838 W/Kg

A.4 MIMO-SAR with Head and Hand Phantom

Prototype A – 859 MHz - 0.25 W accepted power			
$\Delta\varphi=0^o$	$\Delta\varphi=90^o$	$\Delta\varphi=180^o$	$\Delta\varphi=270^o$
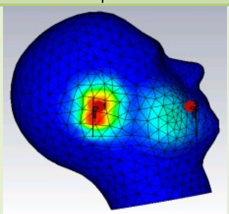	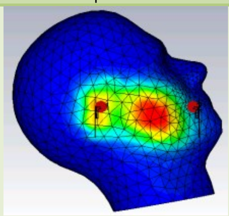	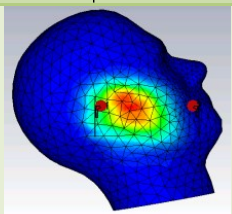	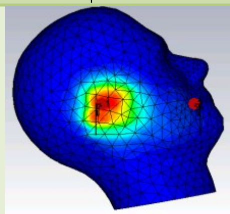
1.355 W/Kg	0.7325 W/Kg	1.27 W/Kg	1.62 W/Kg

Prototype A – 1.92 GHz - 0.13 W accepted power			
$\Delta\varphi=0^o$	$\Delta\varphi=90^o$	$\Delta\varphi=180^o$	$\Delta\varphi=270^o$
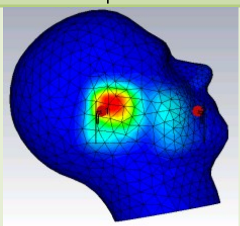	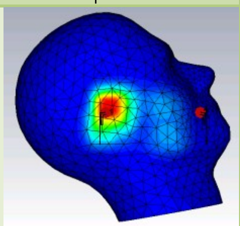	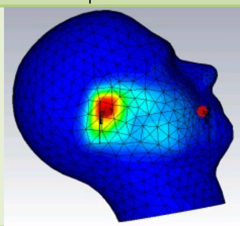	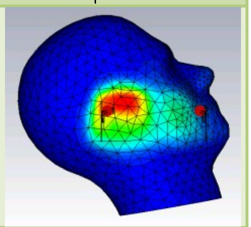
1.0075 W/Kg	1.417 W/Kg	1.0816 W/Kg	0.5941 W/Kg

Prototype B – 859 MHz - 0.25 W accepted power			
$\Delta\varphi=0^o$	$\Delta\varphi=90^o$	$\Delta\varphi=180^o$	$\Delta\varphi=270^o$
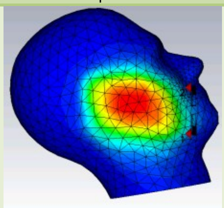	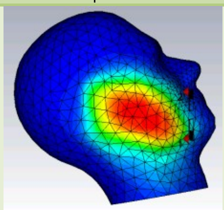	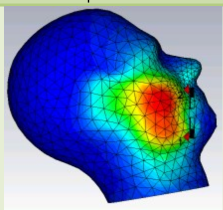	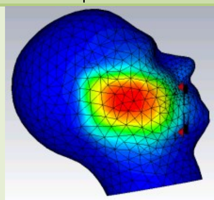
1.165 W/Kg	0.8925 W/Kg	0.46 W/Kg	1.035 W/Kg

Prototype B – 1.92 GHz - 0.13 W accepted power			
$\Delta\varphi=0^o$	$\Delta\varphi=90^o$	$\Delta\varphi=180^o$	$\Delta\varphi=270^o$
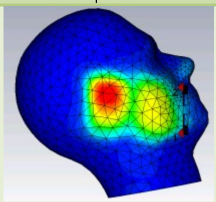	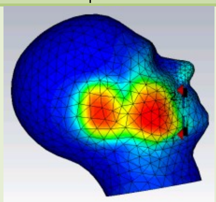	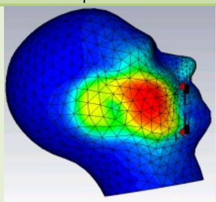	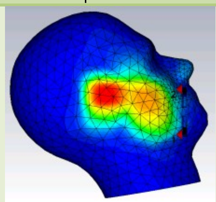
0.7761 W/Kg	0.4056 W/Kg	0.4199 W/Kg	0.7137 W/Kg

Prototype C – 859 MHz - 0.25 W accepted power			
$\Delta\varphi=0^o$	$\Delta\varphi=90^o$	$\Delta\varphi=180^o$	$\Delta\varphi=270^o$
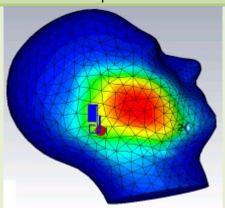	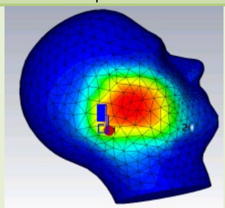	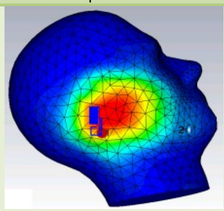	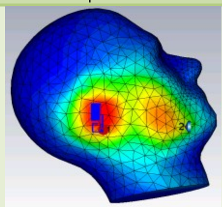
0.895 W/Kg	1.3125 W/Kg	1.2825 W/Kg	0.5475 W/Kg

Prototype C – 1.92 GHz - 0.13 W accepted power			
$\Delta\varphi=0^o$	$\Delta\varphi=90^o$	$\Delta\varphi=180^o$	$\Delta\varphi=270^o$
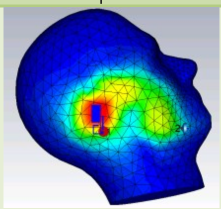	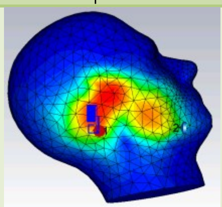	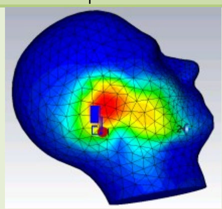	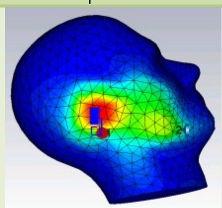
0.6526 W/Kg	0.481 W/Kg	0.5096 W/Kg	0.5525 W/Kg

Prototype D – 859 MHz - 0.25 W accepted power			
$\Delta\varphi=0^o$	$\Delta\varphi=90^o$	$\Delta\varphi=180^o$	$\Delta\varphi=270^o$
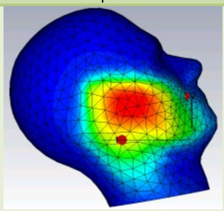	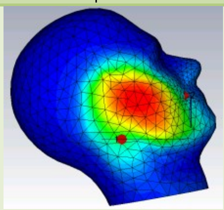	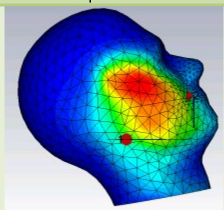	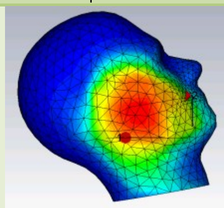
0.585 W/Kg	0.865 W/Kg	0.65 W/Kg	0.395 W/Kg

Prototype D – 1.92 GHz - 0.13 W accepted power			
$\Delta\varphi=0^o$	$\Delta\varphi=90^o$	$\Delta\varphi=180^o$	$\Delta\varphi=270^o$
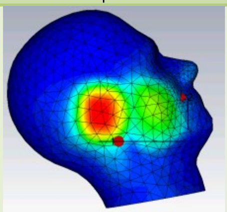	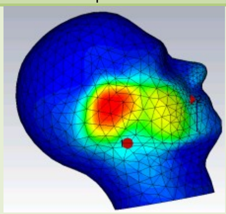	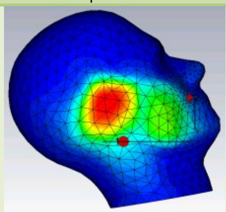	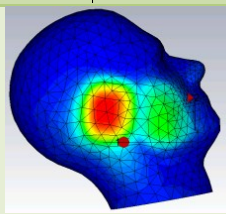
0.5772 W/Kg	0.5161 W/Kg	0.7956 W/Kg	0.8736 W/Kg

http://www.eit.lth.se